New insights into the early Bajocian (Middle Jurassic) carbon cycle perturbation

Baptiste Suchéras-Marx, Guillaume Suan, Fabienne Giraud, Emanuela Mattioli, Hassan M Khozyem, Jean-Charles Mazur, Alicia Fantasia, Jorge E Spangenberg, Thierry Adatte

New insights into the early Bajocian (Middle Jurassic) carbon cycle perturbation

Baptiste Suchéras-Marx[1], Guillaume Suan[2], Fabienne Giraud[3], Emanuela Mattioli[2], Hassan M. Khozyem[4], Jean-Charles Mazur[1], Alicia Fantasia[5], Jorge E. Spangenberg[6], Thierry Adatte[7]

[1] Aix Marseille Univ, CNRS, IRD, INRAE, CEREGE, Aix-en-Provence, France

[2] Université Claude Bernard Lyon 1, ENSL, CNRS, LGL-TPE, 69622 Villeurbanne, France

[3] Univ Grenoble Alpes, Univ Savoie Mont Blanc, CNRS, IRD, Univ Gustave Eiffel, ISTerre, 38000 Grenoble, France

[4] Department of Geology, Faculty of Science, Aswan University, Aswan 81528, Egypt

[5] Department of Geosciences, University of Fribourg, 1700 Fribourg, Switzerland

[6] Institute of Earth Surface Dynamics, University of Lausanne, Géopolis, CH-1015 Lausanne, Switzerland

[7] Institute of Earth Sciences, University of Lausanne, Géopolis, CH-1015 Lausanne, Switzerland

Keywords: early Bajocian, carbon isotopes, carbonate, organic matter, phosphorus, western Tethys

Abstract

Mesozoic strata record numerous negative and positive carbon isotope excursions (CIEs). The Middle Jurassic records a negative ~0.5 ‰ CIE at the Aalenian-Bajocian boundary followed by a positive ~1.5 ‰ CIE covering the entire early Bajocian. Although these CIEs are recorded in northern and southern western Tethys and may reflect perturbations of the global carbon cycle, they remain poorly addressed yet. In this study, we present new geochemical and sedimentological data from the Chaudon-Norante section in France and Murtinheira section in Portugal to better constrain the origin of the lower Bajocian CIEs. Associated with the previously published $\delta^{13}C_{bulk\ carbonate}$ we provide new $\delta^{13}C_{org}$ records, as well as total phosphorus content, phosphorus accumulation rates (AR), and $CaCO_3$ and organic matter data. Contrarily to previous interpretations, our results show no evidence for a carbonate production crisis during the early Bajocian. A slight increase in siliciclastic and phosphorus AR would argue for oceanic fertilization but without a parallel increase in organic matter AR. The obtained stratigraphic $\delta^{13}C_{bulk\ carbonate}$ *vs.* $\delta^{13}C_{org}$ patterns are distinctive and mimic previous box modeling results simulating an increase in productivity forced by higher phosphorus rates from riverine and weathered-carbon input burial. The subsequent organic carbon burial produced

counter-greenhouse conditions, which in turn produced a cooling by CO_2 uptake. Our results indicate that the lower Bajocian event shows several similarities with the late Valanginian positive CIE (also known as Weissert event). An accurate comparison of both events may help for a better understanding of the origin and consequence of such carbon cycle perturbations.

1. Introduction

The Jurassic and Cretaceous strata are punctuated by several positive and negative carbon isotope excursions (CIEs) that have been most often attributed to major climatic, environmental, tectonic and/or biologic perturbations (e.g., Jenkyns et al., 2002; Erba, 2004; Dera et al., 2011; Friedrich et al., 2012). Many of these CIEs mark oceanic anoxic events (OAE), relatively short-lived periods (hundreds of kyr) of widespread oxygen depletion in marine waters although not all of them (e.g., the late Valanginian CIE named Weissert event). Some OAEs are characterized by a negative CIE, like the Toarcian OAE (T-OAE; e.g. Hesselbo et al., 2000; Suan et al., 2010) or the early Aptian OAE (OAE 1a; e.g., Erba and Tremolada, 2004; Westermann et al., 2013). These OAEs were likely initiated by global warming resulting from massive ^{13}C-depleted carbon input such as methane hydrates (Hesselbo et al., 2000), thermogenic methane or volcanic CO_2 (e.g., Larson and Erba, 1999; Suan et al., 2008; Adloff et al., 2020; Matsumoto et al.,2022). In contrast, the Cenomanian-Turonian OAE (OAE 2) is characterized by a marked positive CIE, the widespread occurrence of organic-rich deposits, and oxygen-depleted sedimentary facies (e.g., Schlanger et al., 1987; Bomou et al., 2013). This latter event also likely occurred during a global warming trend (e.g., Friedrich et al., 2012) interrupted by a temporary cooling, possibly driven by increased organic carbon burial (Jarvis et al., 2011) or increased silicate weathering (Pogge von Strandmann et al., 2013; Papadomanolaki et al., 2022). This positive CIE has been classically linked to increased primary productivity and organic carbon burial, removing ^{13}C-depleted organic matter from the oceanic reservoir. The anoxic conditions and organic carbon burial of OAE2 was hence likely initiated by an increase in export productivity that has been linked to a rapid increase in weathering and hence in nutrient input to oceanic waters (Blätter et al., 2011; Monteiro et al., 2012; Pogge von Strandmann et al., 2013) or by increased fertilization from large upwelling areas (Trabucho Alexandre et al., 2010).

Although the geochemical expression of these Mesozoic events is different and evidently associated with either positive or negative CIEs, some events have been more intensively studied. The CIE related to the T-OAE, the Weissert event (late Valanginian) and the OAE 2 have been recorded in many inorganic and organic substrates from various depositional settings, where independent biotic and geochemical proxies have also been generated. In comparison, two CIEs are recorded from lower Bajocian strata and although they may correspond with global lithospheric and volcanism, climatic and biogeochemical perturbations

(e.g. Bartolini and Cecca, 1999; Bartolini and Larson, 2001; Dera et al., 2011), they are relatively under-documented compared to other Mesozoic CIEs. The former event is a ~0.5 ‰ (i.e. per mil) negative CIE documented in several localities close to the Aalenian-Bajocian boundary, as initially shown by Bartolini et al. (1999) who recorded such an excursion in bulk carbonate carbon isotope ($\delta^{13}C$) data from central Italy. More recently, such an event has been also recorded in bulk carbonate $\delta^{13}C$ data from Spain (O'Dogherty et al., 2006), Portugal (Suchéras-Marx et al., 2012), Saudi Arabia and Oman (Al-Mojel et al., 2018), but it is absent in available bulk carbonate $\delta^{13}C$ records in France and Morocco (Suchéras-Marx et al., 2013; Bodin et al., 2017). A negative CIE has also been reported in belemnite calcite in Murtinheira section (Lusitanian Basin, Portugal) and in the Trotternish section (Isle of Skye, Scotland) (Jenkyns et al., 2002), but the Portuguese record has a poor biostratigraphical control (see fig. 7 in Jenkyns et al., 2002) while the negative CIE in the Scottish record is supported by a single data point in the upper part of the section – at the end of the Discites ammonite Zone, earliest ammonite Zone of the Bajocian. Importantly, a >2 ‰, negative CIE is documented in fossil wood (coal and charcoal) from the poorly dated mixed marine and fluvio-deltaic strata putatively attributed to the Aalenian-Bajocian boundary in Yorkshire, UK (Hesselbo et al., 2003), suggesting that the corresponding carbon cycle perturbation has impacted both the oceanic and the atmospheric carbon reservoirs.

The large positive CIE first documented by Corbin (1994) and Bartolini et al. (1996) in the lower Bajocian is better documented. This CIE covers the entire early Bajocian with the positive shift interval corresponding to the Discites (i.e., earliest early Bajocian ammonite Zone) to top of Propinquans (i.e., third early Bajocian ammonite Zone, also called Sauzei) ammonite zones, and the plateau interval covers the whole Humphriesianum ammonite Zone (i.e., fourth and latest early Bajocian ammonite Zone). The return to pre-excursion $\delta^{13}C$ values is recorded in upper Bajocian strata, within the Niortense ammonite Zone (i.e., earliest late Bajocian ammonite Zone). This $\delta^{13}C$ positive excursion is essentially recorded in western Tethys sites, namely in France (Corbin, 1994; Brigaud et al., 2009), Italy (Bartolini et al., 1996; Bartolini et al., 1999), Portugal (Suchéras-Marx et al., 2012), Spain (O'Dogherty et al., 2006; Aguado et al., 2017) and Morocco (Bodin et al., 2017). The $\delta^{13}C$ positive excursion was recently documented in the Arabian platform of the southwestern Tethys (Al-Mojel et al., 2018). This positive CIE was reported in several bulk carbonate records (all above references), of belemnite calcite from the Isle of Skye in Scotland (Jenkyns et al., 2002) and, more recently, of brachiopod calcite from the Murtinheira section in Portugal (Ferreira et al., 2019). However, the lower Bajocian positive CIE has been also recorded in organic carbon material in several localities in Morocco (Bodin et al., 2017; Bodin et al., 2020), therefore bringing new insights into the geographical extent of the carbon cycle perturbation in organic material. The magnitude of the perturbation in bulk carbonate ranges from ~0.5 ‰ in Portugal up to ~3 ‰ in

Saudi Arabia but is comprised between 1 ‰ and 1.5 ‰ in most localities. It ranges about 3 ‰ in organic matter in Morocco, the sole region with such data. This perturbation in the carbon cycle could be linked to a potential decrease in global temperature observed in glendonite records located in high latitudes (Price, 1999; Rogov et al., 2023) or reversely an increase in global temperature based on oxygen isotope data ($\delta^{18}O$) from belemnites (Dera et al., 2011).. This time interval also records important lithospheric changes with the Pacific plate formation (Bartolini and Larson, 2001), the Alpine Tethys opening (Bill et al., 2001), and an accelerated spreading rate in the Central Atlantic (Labails et al., 2010). Finally, this time interval also witnesses an important turnover in ammonite biodiversity (O'Dogherty et al., 2006), a relevant diversification of coccolithophores (Cobianchi et al., 1992; Suchéras-Marx et al., 2015; Giraud et al., 2016) and of dinoflagellate (Wiggan et al., 2017) groups.

The current record of the early Bajocian CIEs is insufficient to develop a satisfactory mechanistic model of the underlying carbon cycle perturbations. In this study, we attempt to document more thoroughly the lower Bajocian carbon isotope composition and sedimentation rates. The results presented here are based on the Chaudon-Norante section (Subalpine Basin, France) and the Murtinheira section at Cabo Mondego (Lusitanian Basin, Portugal) deposits (Fig. 1) using bulk carbonate and organic matter carbon isotopes, phosphorus, calcium carbonate, organic matter, and siliciclastic accumulation rates according to the latest age models. These data are combined with published primary productivity records to discuss the impact of sedimentation rates and phosphorus input on the carbon isotopic composition of both organic and inorganic carbon.

2. Geological settings

2.1. Murtinheira section at Cabo Mondego

The Murtinheira section at Cabo Mondego is located on the Atlantic coast of Portugal near the city of Figueira da Foz in the Lusitanian Basin (Fig. 1A). The Lusitanian Basin was open toward the north, the south and the west and bounded eastward by the Iberian Meseta and the Lusitanian carbonate platform (Fig. 1C-D). This section exposes a key Middle Jurassic succession chosen as the Global Stratotype Section and Point (GSSP) of the Bajocian (Pavia and Enay, 1997) and the Auxiliary Stratotype Section and Point (ASSP) of the Bathonian (Fernandez-Lopez et al., 2009). The section age model is based on ammonite (Ruget-Perrot, 1961; Fernandez-Lopez et al., 1988; Henriques et al., 1994) and nannofossil (Ferreira et al., 2019) biostratigraphy. The studied interval is spanning the uppermost part of the upper Aalenian (Concavum ammonite Zone) to the upper part of the lower Bajocian (Humphriesianum ammonite Zone) and is composed of alternations of limestones and marlstones (Fig. 2). A more exhaustive description of the section is presented in Suchéras-Marx et al. (2012) alongside with the $CaCO_3$ (wt %; i.e. calcium carbonate content in weight

percent) and the bulk carbonate carbon isotope ($\delta^{13}C_{bulk\ carbonate}$) data. A more detailed version of the log is in supplementary material.

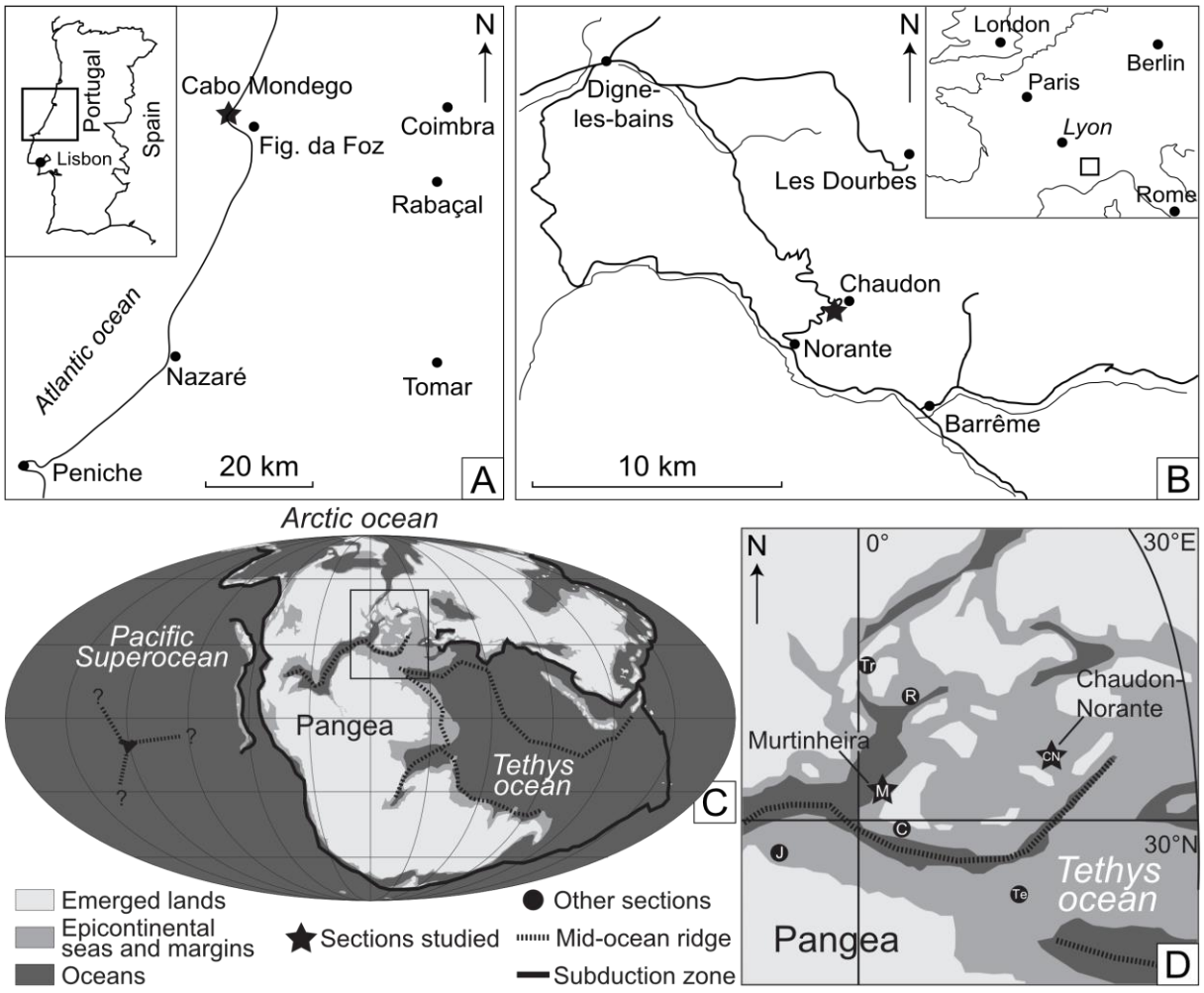

Fig. 1: Location (star) of (A) the Murtinheira section at Cabo Mondego, Portugal and (B) the Chaudon-Norante section, France. C. World paleogeographic map derived from Blakey (2008). D. Western Tethys paleogeographic map derived from Blakey (2008) showing the location of Murtinheira and Chaudon-Norante and of other sections discussed in the text: Tr. Trotternish, Scotland; R. Ravenscar Group composite section, England; C. Casa Blanca, Spain; Te. Terminilletto, Italy; J. Jebel Bou Kendill, Morocco.

2.2. Chaudon-Norante section

The Chaudon-Norante section is located in southeastern France in the Ravin de Coueste near Digne-les-Bains in the Subalpine Basin (Fig. 1B). The French Subalpine Basin was bounded northward by the Jura carbonate platform, westward by the Central Massif and the Ardèche carbonate platform, and southward by the Provence carbonate platform (Fig. 1C-D). Unfortunate candidate for the GSSP of the Bajocian, the Chaudon-Norante section age model is based on ammonite (Pavia, 1983) and nannofossil (Erba, 1990) biostratigraphy. The studied

interval is spanning the uppermost part of the Aalenian (Concavum ammonite Zone) to the upper part of the lower Bajocian (Humphriesianum ammonite Zone) and is composed of alternations of limestones and marlstones / calcareous to argillaceous marlstones (Fig. 3). A more exhaustive description of the section is presented in Suchéras-Marx et al. (2013) alongside with the $CaCO_3$ (wt %) and the $\delta^{13}C_{bulk\ carbonate}$ data. A more detailed version of the log is in supplementary material.

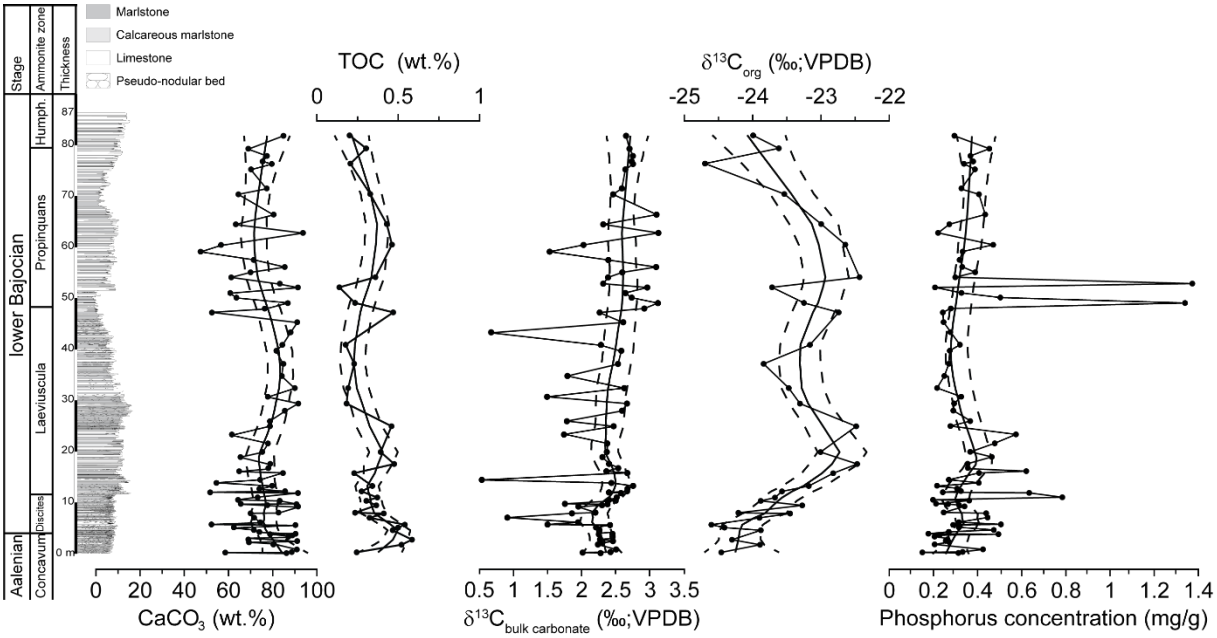

Fig. 2: Stratigraphic variations of $CaCO_3$ (wt %), TOC (wt %), $\delta^{13}C_{bulk\ carbonate}$ (‰ VPDB), $\delta^{13}C_{org}$ (‰ VPDB) and phosphorus concentration (mg/g) in the Murtinheira section.

3. Analytical methods and calculation

3.1. Organic matter analysis: TOC, $\delta^{13}C_{org}$ and palynofacies

A total of 80 samples (32 samples from Murtinheira and 48 samples from Chaudon-Norante) were analyzed for their total organic carbon (TOC) contents and carbon isotope composition of organic matter ($\delta^{13}C_{org}$). The analyzed samples correspond to limestones, argillaceous limestones, calcareous marlstones, marlstones or argillaceous marlstones. Prior to analysis, around 500 mg of powdered bulk sediment was mixed in 2 mL of distilled water and 5 to 8 mL of 2N HCl and reacted overnight at ambient temperature to remove calcium carbonate. The residue was rinsed with distilled water and centrifuged twice to remove the supernatant, reacted again with 2 mL of distilled water and 5 to 8 mL of 2N HCl and left overnight in a 90-95°C water bath to remove more refractory inorganic carbon phases. The residue was finally rinsed three times with distilled water to reach neutrality and oven-dried at 50°C.

The TOC was measured by gas chromatography using an elementary analyzer Thermo-Finnigan Flash EA 1112 at the Université de Lausanne, Switzerland. The TOC is expressed in

weight percent of the rock analyzed (wt %) and the uncertainty is about 0.1 wt %. The carbon isotopic ratio $\delta^{13}C_{org}$ was measured using a Thermo Fischer Scientific Delta V Plus isotope ratio mass spectrometer at the Université de Lausanne, Switzerland. Each sample was analyzed once. The results were standardized using Glycine (14 analyses; 2σ = 0,22 ‰; standard value -26.11 ‰), Urea (13 analyses; 2σ = 0,5 ‰; standard value -43.13 ‰), Graphite-24 (6 analyses; 2σ = 0,64 ‰; standard value -16.05 ‰) and Pyridine (6 analyses; 2σ = 2,78 ‰; standard value -29.20 ‰) and are expressed in per mil Vienna Pee Dee Belemnites (‰ VPDB). Eight samples – four from each site – were prepared in order to determine the source of the organic matter. About 1 cm^3 of powdered rock was dissolved in HCl 37% for 4h then in HF 70% for 12 h. Then, the preparation was rinsed with ~80°C HCl 37% and 80°C KOH 10% was added to the preparation for 10 min. The preparation was centrifugated at 3200 t/min for 7 min, sieved at 150 µm and mounted between slide and cover slide. Observations were made on an optical microscope without polarization.

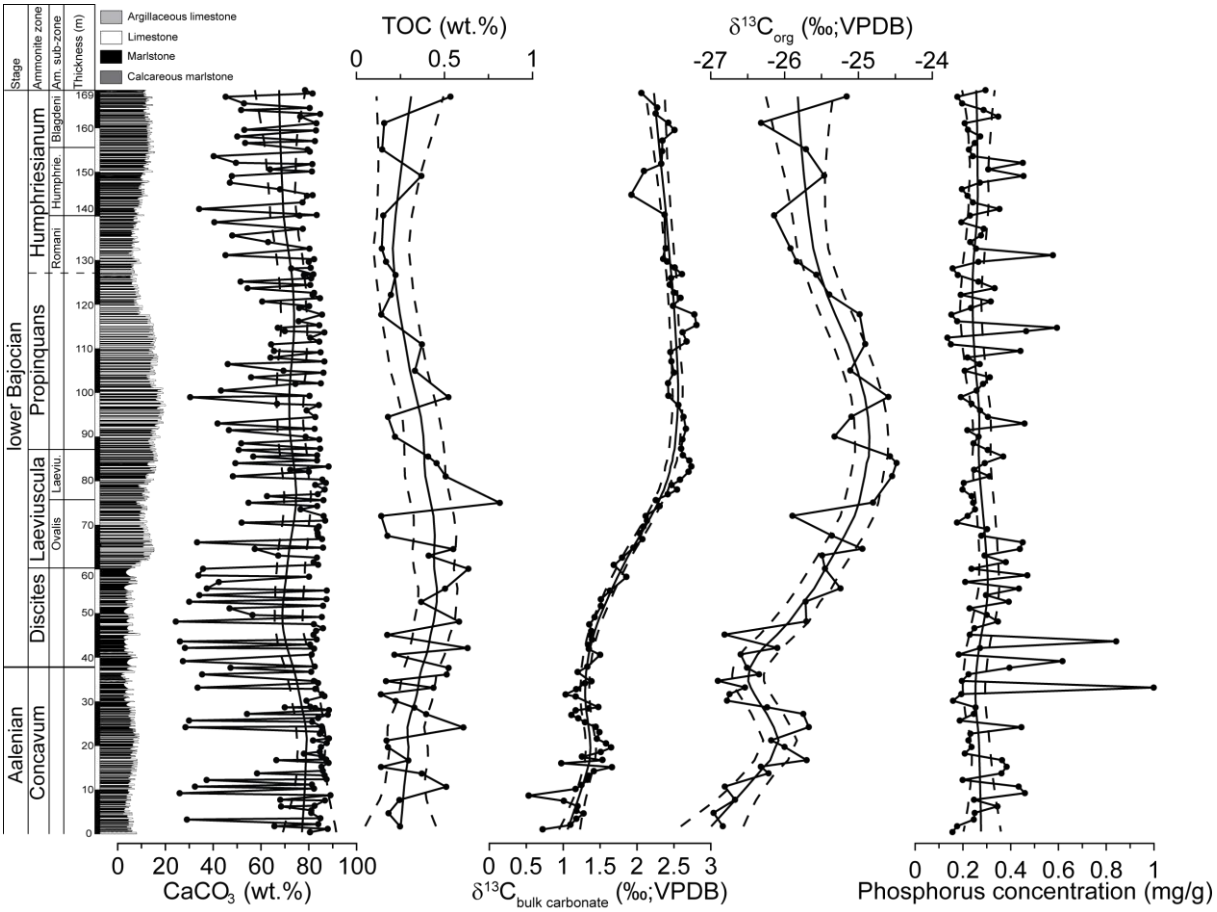

Fig. 3: Stratigraphical variations of $CaCO_3$ (wt %), TOC (wt %), $\delta^{13}C_{bulk\ carbonate}$ (‰ VPDB), $\delta^{13}C_{org}$ (‰ VPDB) and phosphorus concentration (mg/g) at Chaudon-Norante.

3.2. Total phosphorus content

A total of 193 samples (79 samples from Murtinheira and 114 from Chaudon-Norante) were analyzed for their total phosphorus contents (P_{tot}) using the ascorbic acid method (Mort et al., 2007). About 100 mg of powdered bulk sediment for each sample was first dried at 45°C. Once dry, 1 mL of $MgNO_3$ was mixed to the samples and heat in a furnace at 550°C for 2 hours. Once cooled, the residue was reacted with 10 mL of 1N HCl for 16 h under constant shaking. The solution was filtered with a 63 μm filter and diluted 10 times. The filtered solution was then mixed with ammonium molybdate and potassium antimonyl tartrate forming phosphomolybdic acid. This acid was reduced with ascorbic acid forming a deep blue liquid. The total phosphorus content depends on the intensity of the blue color, which was measured using a Perkin Elmer UV/Vis Spectrophotometer Lambda 25. The concentration of PO_4 was determined by calibration with standard solutions (BD47 and NU81) with known concentration, is expressed in mg/g.

3.3. Accumulation rates

Using available $CaCO_3$ data for both sections (from Suchéras-Marx et al., 2012; 2013; 1 sigma ~1 wt %) and TOC and P_{tot} quantified in this study, a set of derived accumulations rates (AR; g/m^2/a) were calculated. Sedimentation rates (SR; m/Ma) were determined using the astrochronological time scale previously obtained at Chaudon-Norante by Suchéras-Marx et al. (2013; alternative solution based on Gradstein et al. 2020 in supplementary data). SR was computed at the scale of ammonite zones in order to apply the same calculation in both Chaudon-Norante and Murtinheira. The calculated variables are the $CaCO_3$ AR, Siliciclastic AR, C_{org} AR and PAR (i.e., phosphorus AR). C_{org} AR was calculated based on TOC, whereas Siliciclastic AR is calculated as the residues of the sum of $CaCO_3$ AR and C_{org} AR. The dry bulk rock density was calculated based on the $CaCO_3$ (wt %)/Density linear relation established in both sections by Suchéras-Marx et al. (2014):

$[CaCO_3] \times SR \times Density = CaCO_3\ AR$

$[TOC] \times SR \times Density = C_{org}\ AR$

$P_{tot} \times SR \times Density = PAR$

$(1 - [CaCO_3] - [TOC]) \times SR \times Density = Siliciclastic\ AR$

In order to show trend in $CaCO_3$ (wt %), TOC (wt %), $\delta^{13}C_{bulk\ carbonate}$ (‰ VPDB), $\delta^{13}C_{org}$ (‰ VPDB), P_{tot} (mg/g) and accumulation rates results, LOESS-smoothed curves (smoothing factor of 0.3) and the 95%CI (dashed lines) were calculated using PAST3 (Hammer et al., 2001) and presented in figures 2-4-5-6.

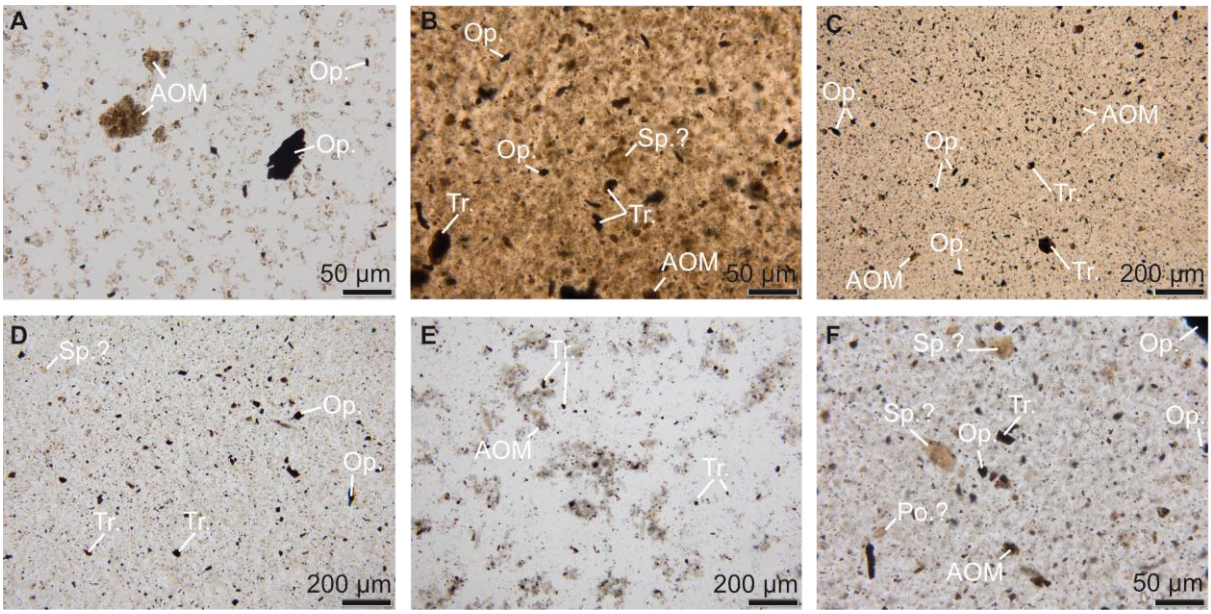

Fig. 4: Photomicrographs of some representative organic components of the Chaudon-Norante (A-C) and Murtinheira (D-F) sections. AOM = Amorphous Organic Matter; Op. = Opaque phytoclasts; Po. = pollen; Sp. = spores; Tr. = translucent phytoclasts. A. sample CN1810; B. sample CN500; C. CN1990; D. CM70; E. CM67; F. CM31.

4. Results

4.1. Relative concentrations and isotopic records

4.1.1. The Murtinheira section (Fig. 2)

The TOC values at Murtinheira are very low, ranging from 0.14 to 0.58 wt %, and show a general decreasing trend stratigraphically upwards, with the highest values recorded near the Aalenian-Bajocian boundary. The lower part of the Laeviuscula ammonite Zone records few higher values around 0.5 wt %, whereas minimum values are recorded in the middle and upper part of the Laeviuscula ammonite Zone. Overall, TOC and $CaCO_3$ contents (Figs. 2 and 3) are negatively correlated (Chaudon-Norante r=-0.87; Murtinheira r=-0.73), and TOC is very low, indicating that TOC values are mostly controlled by a variable dilution by $CaCO_3$ contents.

The $\delta^{13}C_{org}$ values range between −22.4 ‰ and −24.7 ‰, with the lowest values occurring in the Concavum and lower part of the Discites ammonite zones, and maximum value occurring in the Propinquans ammonite Zone. The $\delta^{13}C_{org}$ values increase markedly by about ~2 ‰ across the transition between the Discites–Laeviuscula ammonite zones and decrease down to −24.7 ‰ at the end of the Propinquans ammonite Zone. The overall pattern can be described as a ~2 ‰ positive CIE from the Concavum to the Propinquans ammonite Zone, interrupted by a ~1 ‰ negative CIE in the upper part of Laeviuscula ammonite Zone, and followed by a second ~1 ‰ negative CIE in the upper part of the Propinquans ammonite Zone. Based on organic matter observations of 8 samples in light microscopy (Fig. 4), the

palynomorphs at Murtinheira are dominated by opaque phytoclasts, with subordinate amounts of translucent phytoclasts, rare terrestrial sporomorph (spore and pollen grains) and rare marine palynomorphs (dinoflagellate cysts).

The P_{tot} concentrations record markedly different stratigraphic patterns. Most values are comprised between 0.2 and 0.5 mg/g, except few samples recording higher concentration (up to 1.37 mg/g). The exceptional high concentration values may be linked to local fish scales accumulation although this hypothesis is not tested. The smoothed P_{tot} profile shows two intervals of increasing values within the Discites ammonite Zone and in the lower part of the Laeviuscula ammonite Zone. Phosphorus contents decrease down to around 0.3 mg/g in the middle part of the Laeviuscula ammonite Zone and increase gradually up to almost 0.4 mg/g in the lowermost part of the Humphriesianum ammonite Zone. The P_{tot} shows a poor linear correlation with $CaCO_3$ or TOC contents (r = −0.03; Fig. 5).

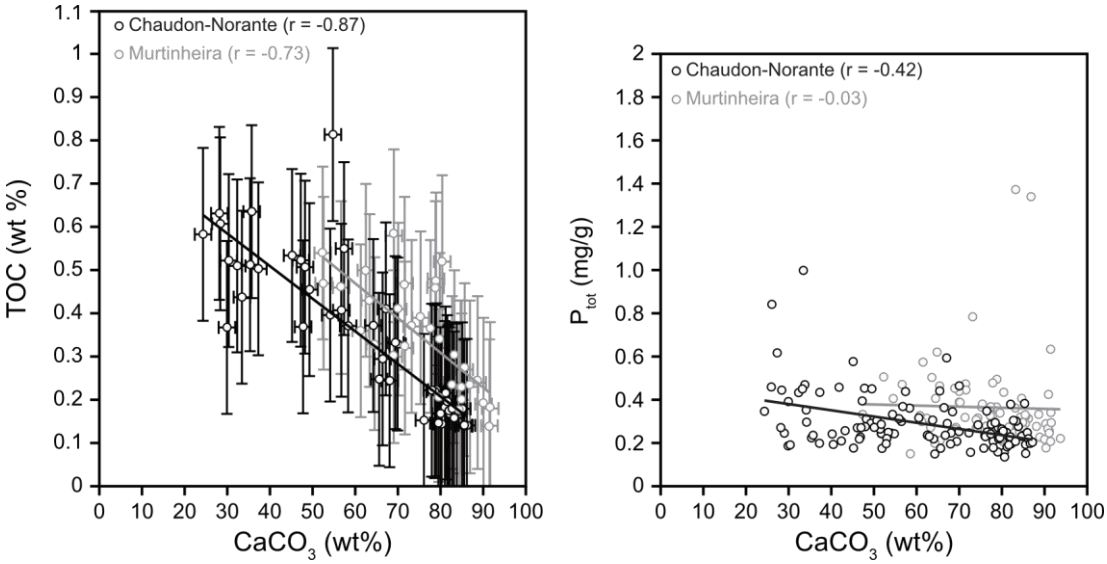

Fig. 5: $CaCO_3$ (wt %) *versus* TOC (wt %) plot (left-hand side) and $CaCO_3$ (wt %) *versus* P_{tot} (mg/g) plot (right-hand side) with Chaudon-Norante samples in black and Murtinheira samples in grey. There is a clear negative linear correlation between $CaCO_3$ and TOC values, with marlstones being more enriched in organic carbon. However, TOC values are low suggesting important effect of measurement uncertainties which are about 0.1 wt % (1σ). There is no relationship between $CaCO_3$ and P_{tot} values at Murtinheira, whereas a moderately good negative linear correlation is apparent for Chaudon-Norante, with marlstones being slightly enriched in P_{tot}.

4.1.2. The Chaudon-Norante section (Fig. 3)

At Chaudon-Norante, TOC contents are comparable to Murtinheira with values ranging from 0.14 wt % to 0.81 wt %. The TOC contents have higher concentrations in marlstones than in limestones (Figs. 3 and 5). The phosphorus concentration is ranging between 0.1 and

0.5 mg/g, with the exception of few samples reaching almost 1 mg/g. Both the raw and smoothed P_{tot} profiles show a slight increase around the Discites-Laeviuscula ammonites zones boundary (Fig. 3). The P_{tot} shows a moderately good negative linear correlation with $CaCO_3$ contents ($r = -0.42$) but there are no clear stratigraphic trends.

The $\delta^{13}C_{org}$ values range between −24.5 ‰ and −27 ‰, with the lowest values occurring in the Concavum ammonite Zone and the highest values occurring in the upper part of the Laeviuscula ammonite Zone (Fig. 3). The $\delta^{13}C_{org}$ profile shows a first increasing trend within the Concavum ammonite Zone interrupted by a negative CIE around the Aalenian-Bajocian boundary, values increase again by 2 ‰ in the Discites and Laeviuscula ammonite zones up to a maximum around the Laeviuscula-Propinquans ammonite zones boundary. The $\delta^{13}C_{org}$ values then decrease up to the top of the section, thus forming a broad, 2 ‰ positive CIE, but do not reach pre-excursion values (Concavum ammonite Zone and at the Aalenian-Bajocian boundary). Based on organic matter observations of 8 samples in light microscopy (Fig. 4), the palynomorphs at Chaudon-Norante are dominated by phytoclasts (opaque and translucent) and amorphous organic matter, with rare terrestrial sporomorphs (spore and pollen grains) and marine palynomorphs.

4.2. Accumulation rates

4.2.1. The Murtinheira section (Fig. 6)

The SR determined at the ammonite zone level show the lowest values of ~ 11.5 m/Myr in the Discites Zone. This interval is also marked by low wt % $CaCO_3$, resulting in an important drop in $CaCO_3$ AR. The low PAR reflects the decrease in sedimentation rate despite the increase in phosphorus concentration. The Laeviuscula Zone conversely corresponds to the highest sedimentation rates. Hence, all sedimentary fractions considered here are increasing in terms of accumulation rates. However, only $CaCO_3$ AR is very high all along the latter ammonite zone. The siliciclastic AR, C_{org} AR and PAR show a peak in the lower part of the Laeviuscula ammonite Zone. Finally, two distinct patterns are observed in the Propinquans ammonite Zone. The $CaCO_3$ and phosphorus ARs tend to increase between the base and the top of the latter ammonite zone. Conversely, siliciclastic and C_{org} ARs tend to decrease between the base and the top of this ammonite zone. Overall, siliciclastic and C_{org} ARs have very similar trends and $CaCO_3$ is the most important sediment component in term of accumulation rates. Finally, C_{org}/P_{tot} (molar ratio) is always below the Redfield ratio 1:106. Alternative results using Gradstein et al. (2020) age model is presented in supplementary material (Supplementary fig. 1). This solution is not described in this study.

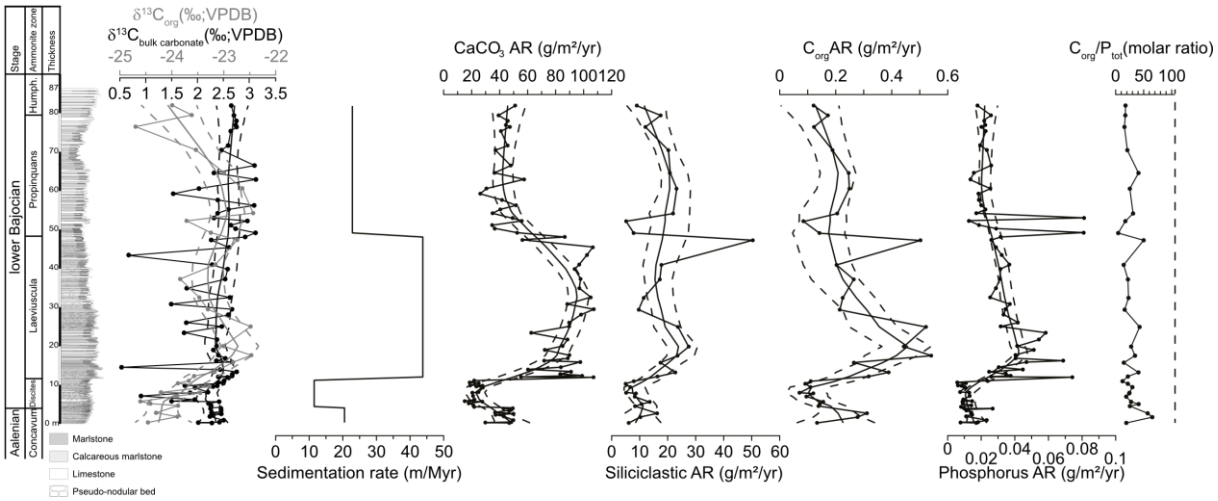

Fig. 6: Stratigraphic changes in sedimentation rate at Murtinheira (based on Suchéras-Marx et al., 2013 age model) and the resulting $CaCO_3$ accumulation rates (AR; g/m²/a), Siliciclastic AR (g/m²/a), C_{org} AR (g/m²/a), and phosphorus AR (g/m²/a), along the C_{org}/P_{tot} molar ratio. The dashed line in C_{org}/P_{tot} data corresponds to the Redfield ratio (1:106).

4.2.2. The Chaudon-Norante section (Fig. 7)

The age model for the lower Bajocian from Suchéras-Marx et al. (2013) was built on the astrochronology of the Chaudon-Norante section. Nevertheless, to compare both sections with the same resolution, sedimentation rates are also calculated per ammonite zone (Fig. 7). The sedimentation rates are relatively stable all along the section with a slight decrease in the Propinquans ammonite Zone which is the interval with rare marlstone beds. The $CaCO_3$ AR is the highest sediment influx even if the clay-rich beds have in some cases a higher siliciclastic AR. As observed in the Murtinheira section, siliciclastic and C_{org} ARs have similar trends with a maximum in the Discites ammonite Zone and a slight increase in the upper part of the Humphriesianum ammonite Zone. Excepted few points, the end of the Concavum ammonite Zone corresponds to a slight decrease in phosphorus accumulation rates whereas the Discites ammonite Zone corresponds to a slight increase. C_{org}/P_{tot} (molar ratio) is always below the Redfield ratio 1:106. Similar to the Murtinheira section, alternative results using the Gradstein et al. (2020) age model are presented in supplementary material (Supplementary fig. 2). This solution is not described in this study.

5. Discussion

5.1. The lower Bajocian negative excursion record

The Aalenian-Bajocian boundary is characterized in many sections by a negative CIE (Bartolini et al., 1996; Hesselbo et al., 2003; O'Dogherty et al., 2006; Fantasia et al., 2022). This event is clearly recorded by a 0.5 ‰ negative CIE across the Aalenian-Bajocian in the $\delta^{13}C_{org}$ profile at Chaudon-Norante (Fig. 3) and in Morocco (Fig. 8; Bodin et al., 2017; 2020), but not at

Murtinheira (Fig. 2). Conversely, the CIE is hardly discernable in bulk carbonate in Chaudon-Norante and in Moroccan sites (Fig. 8), but well-expressed at Murtinheira (Figs. 2 and 8) in the lower part of the Discites ammonite Zone. Discussing the possible causes of this carbon isotope event is thus complex due to its patchy record in the different localities and carbon substrates. The negative CIE is clearly short-lived and has a lower amplitude than the following positive CIE (Bartolini et al., 1996; O'Dogherty et al., 2006; Suchéras-Marx et al., 2013). The low magnitude and relatively short duration of this negative CIE may thus partly explain its uneven occurrence among different sites and various types of investigated material. For instance, relatively small changes in proportion of isotopically distinct OM and $CaCO_3$ sources may produce large changes in bulk organic and inorganic records (Swart and Eberli, 2005; Suchéras-Marx et al., 2012; Suan et al., 2015) and may thus have blurred either ways this small negative CIE in some Aalenian-Bajocian bulk records.

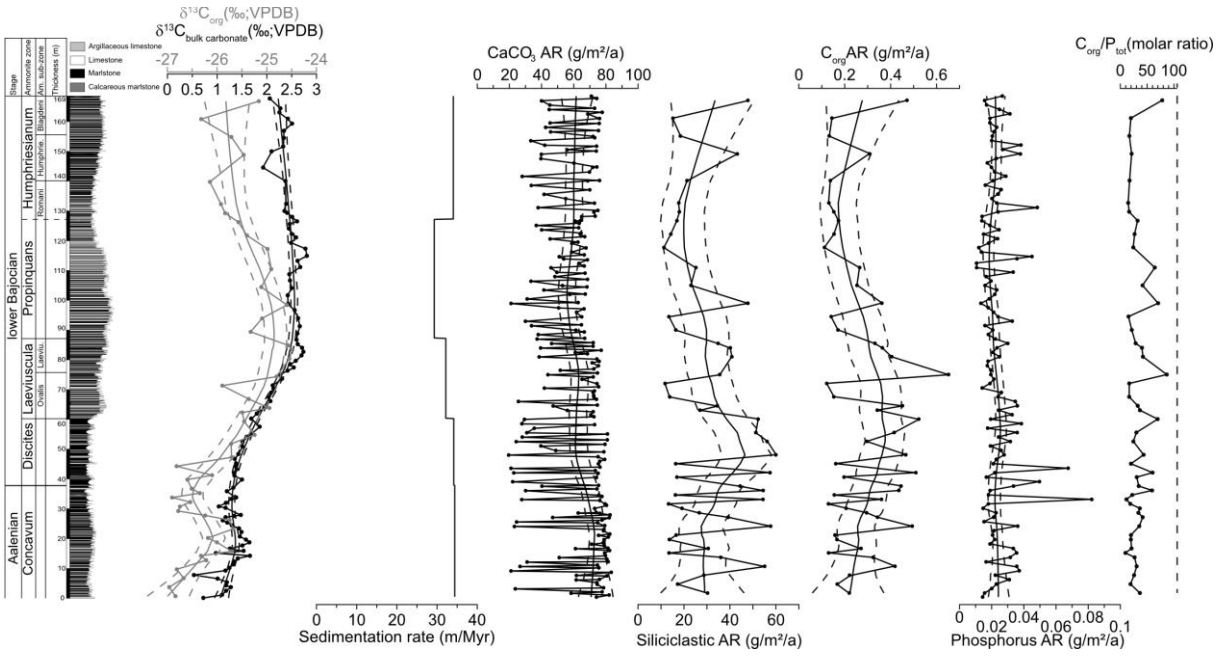

Fig. 7: Stratigraphic changes in sedimentation rate at Chaudon-Norante (based on Suchéras-Marx et al., 2013 age model) and the resulting $CaCO_3$ accumulation rates (AR; g/m²/a), Siliciclastic AR (g/m²/a), C_{org} AR (g/m²/a), and phosphorus AR (g/m²/a), along the C_{org}/P_{tot} molar ratio. The dashed line in C_{org}/P_{tot} data correspond to the Redfield ratio (1:106).

5.2. The lower Bajocian positive excursion record

Our new carbon isotope records support that the Bajocian positive CIE occurs in organic material in both Portugal (Fig. 2) and SE France (Fig. 3). Such an occurrence strongly suggest that this geochemical anomaly reflects a perturbation of the global exchangeable carbon reservoir. Indeed, if the positive CIE was only recorded in $\delta^{13}C_{bulk\ carbonate}$, it could have reflected a global shift in the carbonate production i.e., by change in the $CaCO_3$ producers with more

positive $\delta^{13}C$ signature (Suchéras-Marx et al., 2012). Conversely, if the $\delta^{13}C_{org}$ positive CIE was recorded only in Morocco (Bodin et al., 2017; 2020), local effect like the carbon residence time in the carbonate platform, or local changes in hydrology, or even change in the source and preservation of the organic matter may have been involved (Suan et al., 2015). Our concomitant record of a positive CIE in both $\delta^{13}C_{bulk\ carbonate}$ and $\delta^{13}C_{org}$ dismisses these hypotheses and confirms the large geographical extent of this carbon cycle perturbation. Our new data suggest that the magnitude of the shift ranges between 1 ‰ and 1.5 ‰, in line with previous bulk organic and inorganic records, as well as brachiopod (Ferreira et al., 2019) and belemnite (Jenkyns et al., 2002) records. These latter records have an inherently low resolution and may therefore not fully capture short scale variations in $\delta^{13}C$. Also, changes in proportions of various inorganic and organic particles with distinct $\delta^{13}C$ signatures may greatly distort bulk sediment records (Swart and Eberli, 2005; Suchéras-Marx et al., 2012; Suan et al., 2015). The preliminary qualitative palynological investigations of samples show no major changes in the dominant kerogen type in each section, indicating that the recorded trends are not attributable to changing contribution of distinct type of organic carbon. Nevertheless, our observations indicate that the kerogen is dominated by terrestrial opaque phytoclasts at Murtinheira, whereas phytoclasts and amorphous organic matter (AOM) dominate at Chaudon-Norante (Fig. 4). Traditionally, structureless AOM has been considered as derived from bacteria or phytoplankton and strongly altered macrophyte remains (Pacton et al., 2011), this latter source being a volumetrically secondary component in marine sediments (Tyson, 1995). The distal position of the site and non-gelified aspect of the AOM at Chaudon-Norante could therefore indicate a marine source, which was ^{13}C-depleted by 2-4 ‰ compared to terrestrial phytoclasts during the Jurassic (Suan et al., 2015). Such a ^{13}C-depletion is in good agreement with the 2 ‰ offset toward lower values of the Chaudon-Norante $\delta^{13}C_{org}$ record relative to that at Murtinheira (Figs. 2, 3 and 8). Accordingly, the $\delta^{13}C_{org}$ record at Chaudon Norante, where ^{13}C-depleted AOM kerogen occurs in higher proportions, may capture a mixed terrestrial-marine signal, whereas the Murtinheira record, where phytoclasts dominate, may essentially capture a terrestrial signal. Such palynological observation are preliminary and qualitative, and further quantification of changing proportions of various inorganic and organic carbon sources are required to more robustly assess the magnitude of the lower Bajocian positive CIE using bulk records.

5.3. Similarities with other Mesozoic CIEs

The triggers of the CIEs might be interpreted differently according to their inferred timescales. According to Gradstein et al. (2020), the $\delta^{13}C$ increase interval is more or less concomitant with the whole Discites and Laeviscula ammonite zones thus corresponding to 580 kyr, and the plateau is lasting 580 kyr. The increasing phase and the plateau have thus the same

duration and the whole perturbation lasts a little longer than one million years. The duration of ammonite zones is roughly estimated based on the assumption of an equal duration of subzones and thus it is dependent on the number of subzones in the sub-Boreal zonation scheme (Gradstein et al., 2020). The cyclostratigraphic study of Ikeda et al. (2016) indicates a total duration of ~4 Myr for the Bajocian-Callovian interval, but no other biostratigraphic information is available for the condensed radiolarites section they studied. This poor biostratigraphic age control makes the former results difficult to consider in our framework. According to the cyclostratigraphy established by Suchéras-Marx et al. (2013) at Chaudon-Norante, the positive isotope shift lasted 1.357 Myr (i.e., from Concavum-Discites boundary to almost the end of the Laeviuscula ammonite Zone) and the plateau lasted 2.724 Myr (i.e., from almost the end of the Laeviuscula ammonite Zone to the end of the Humphriesianum ammonite Zone) for a total of 4.082 Myr, thus approximately 4 times longer than the duration stated in Gradstein et al. (2020). These differences in the time estimation of the early Bajocian are critical and further data are necessary to definitively get to a consensual solution.

Following the timescale of Suchéras-Marx et al. (2013), the duration of the positive carbon isotope excursion is similar to that of the Weissert event (lasting some 5.84 Myr starting from the increasing $\delta^{13}C$ values up to the middle of a plateau within recovery $\delta^{13}C$ values; Martinez et al., 2015) and much longer than other Mesozoic carbon isotope excursions associated with OAEs, which last around ~1 Myr (e.g., T-OAE, Ait-Itto et al., 2018; OAE1a, Malinverno et al., 2010; OAE2, Boulila et al., 2020) although the exact timescale of those events is still debated (e.g., T-OAE, Suan et al., 2008; Huang and Hesselbo, 2014; Ruebsam et al., 2014; OAE2, Voigt et al., 2008; Ma et al., 2014; Eldrett et al., 2015). The negative excursion at the Aalenian/Bajocian boundary based on $\delta^{13}C_{org}$ data is estimated to last between 520 kyr and 570 kyr (i.e., 27 cycles of 20 ka or 14 cycles of 37 ka or 41 ka or 5 cyles of 100 ka and 3 cyles of 20 ka). Such a duration seems incompatible with a short-lived event such as methane clathrates release (e.g., Dickens et al., 1995).

Thus, the carbon isotope perturbations can be described as a ~550 ka negative excursion followed by a positive CIE composed of a phase of increasing values lasting 2.5 times longer than the negative excursion, but shorter than the plateau phase; and a plateau phase ~2 times longer than the increasing phase. The Aalenian-Bajocian negative CIE observed in several (although not all) records likely reflects a relatively short-lived carbon cycle perturbation, whereas the lower Bajocian positive CIE recorded in bulk carbonate, fossil calcite and organic matter is one of the most pronounced and long-lived carbon cycle perturbations of the Jurassic Period.

Altogether, the long, cumulated duration of the two CIEs is compatible with long-lived geological perturbations, such as tectonically-controlled climatic (e.g., global tectonic,

volcanism like large igneous province) or oceanographic changes (e.g., oceanic gateways). The possible mechanisms involved are discussed in the following section.

5.4. Possible environmental drivers of the early Bajocian positive excursion

5.4.1. Higher fertility and enhanced organic matter burial

Positive CIEs in the geological record have been classically attributed to the increased burial of ^{13}C-depleted organic carbon in the oceans, thereby increasing the carbon isotopic composition of dissolved inorganic carbon ($\delta^{13}C_{DIC}$) values (e.g., Vincent and Berger, 1985; Schlanger et al., 1987). This increased organic carbon burial could reflect higher organic matter production and supply or enhanced preservation in the sediment favored by anoxic conditions. This scenario is partly compatible with some key features of Bajocian record, despite the fact that no black shales are observed in this study. Indeed, the lower Bajocian strata record some of the most important biotic events of the Mesozoic plankton revolution, notably the diversification of the major coccolithophores genus *Watznaueria* (Cobianchi et al., 1992; Giraud et al., 2016), the emergence of planktic foraminifera (BouDagher-Fadel, 2015), an increase in abundance of the dinoflagellate genus *Dissiliodinium* (Wiggan et al., 2018), an increase in calcareous nannofossil accumulation rates (Suchéras-Marx et al., 2015) and calcareous nannoplankton-derived $CaCO_3$ (Suchéras-Marx et al., 2012). In parallel, an increase in the geographical distribution of radiolarian deposits is documented (Bartolini et al., 1999) although a major radiolarian turnover is dated earlier in the middle-late Aalenian (Bartolini et al., 1999; Aguado et al., 2008). The early Bajocian is also associated with a major ammonite turnover (O'Dogherty et al., 2006). Moreover, abundant bioclastic deposits of crinoids and bivalves in carbonate platforms in France and Spain point to the dominance of a filtering community in neritic environments, hence to nutrient-rich surface waters (Dromart et al., 1996; Thiry-Bastien, 2002; Aurell et al., 2003; Brigaud et al., 2009; Molina et al., 2018). Finally, the Chaudon-Norante succession records abundant *Zoophycos* that likely also reflects higher organic matter influx to the sediment (Olivero, 1994). Overall, these paleontological data suggest that strata recording the lower Bajocian positive CIE were deposited during an interval of increased primary productivity. Such an important increase in productivity would have been logically sustained by higher siliciclastic and phosphorus inputs from weathering or increase of widespread upwelling in the western Tethys. The former hypothesis is in line with the major rise of siliciclastic AR and PAR recorded at Murtinheira (Fig. 6), but at odds with the Chaudon-Norante data (Fig. 7) showing a little increase in both siliciclastic AR and C_{org} AR and almost no change in PAR, along with a relative low increase in Nannofossil AR. Thus, even if paleontological data suggest a high primary productivity during the early Bajocian, a model of fertilization triggered by continental weathering does not seem fully compatible with the new sedimentological and geochemical data presented here. However, this fertilization model

cannot be fully ruled out due to the limited number of sites studied. Conversely, the fertilization could be related to upwelling development in the western Tethys. However, our data cannot unambiguously discriminate between the upwelling and other mechanisms of ocean fertilization. According to a previous study on radiolarites, the Western Tethys and Alpine Tethys did not see the development of upwelling-related high productivity, and information from North Atlantic sites is not available (Baumgartner, 2013).

The lower Bajocian successions investigated in this paper and in previous works (Raucsik, 1999; Bodin et al., 2020) have low to very low TOC contents and C_{org} AR (Figs. 2, 3, 6 and 7). Furthermore, lower Bajocian strata are unnoticeable in terms of occurrence of petroleum source rock (Kendall et al., 2009). Nevertheless, a stratigraphically thin (~10 cm) black shale level ('Gaetani level') at Alpe Turati in Italy has been reported (Erba et al., 2019), which may stratigraphically correspond to part of the increasing phase of the positive CIE. Moreover, "black flysch" deposits have been dated as early Bajocian in Poland, and lower Bajocian black shales have been reported in Alaska (Imlay, 1976; Barski et al., 2012). To our knowledge, however, the lower Bajocian strata do not yield widespread black shales levels. Importantly, the C_{org}/P_{tot} molar ratios in both studied sites are always lower than the Redfield ratio 1:106 (Figs. 6 and 7), which suggest overall stable, oxic conditions throughout the deposition of the corresponding strata (Suan et al., 2012). This is also coherent with geochemical results from La Losillas section in Spain, which suggest fluctuating but overall oxic conditions during the early Bajocian (Molina et al., 2018). Although investigation of oxygenation conditions and rates of carbon burial at extra-Tethyan sites is warranted, all these data are thus at odds with the hypothesis of increased organic matter preservation under low oxygenation as the main trigger of the Bajocian CIEs, as proposed for some comparable negative and positive CIEs associated with OAEs.

5.4.2. Carbonate crisis

Alternatively, the positive CIE could be related to a major neritic carbonate crisis, which would have decreased the burial of relatively ^{13}C-enriched material (Bartolini and Cecca, 1999; Bodin et al., 2017). This hypothesis is not supported by our new records showing no major decrease in $CaCO_3$ AR in both sections studied here (Figs. 6 and 7; regardless of the age model used, see SupplFigs. 1-2; Gradstein et al., 2020). However, the carbonate factory was dominated by neritic production by the Middle Jurassic (Suchéras-Marx et al., 2012) thus by carbonate platforms. Hence, the state of productivity in such environments is more critical to evaluate the impact of carbonate burial on the lower Bajocian carbon cycle. In eastern France, the early Bajocian was a period an intermediate $CaCO_3$ accumulation rates (Dromart et al., 1996). A published compilation of carbonate platforms sedimentation rates does show a limited carbonate crisis (Andrieu et al., 2016). The Bajocian seems to be an intermediate state

between an Aalenian (or upper Aalenian) low carbonate production state and an upper Bajocian high state (Dromart et al., 1996; Andrieu et al., 2016; Fantasia et al., 2022). This crisis, first proposed on the basis of observations from carbonate platforms in Italy (Bartolini and Cecca, 1999), is indicated by a reduction in $CaCO_3$ accumulation rates in the High Atlas of Morocco (Bodin et al., 2017) and Provence platform of SE France (Léonide et al., 2007). In those regions and in many other carbonate platforms, abundant crinoids and, to a lesser extent, other filtering organisms are common to dominant carbonate producers during the early Bajocian (e.g. Burgundy-Ardèche, France, Dromart et al., 1996; Lusitanian basin, Portugal, Azerêdo, 1998; Jura, France, Thiry-Bastien, 2002; Basque-Cantabrian and Iberian basins, Spain, Aurell, 2003; Betic basin, Spain, O'Dogherty et al., 2006; Molina et al., 2018; United Arab Emirates, Hönig and John, 2015; northwestern Paris basin, France, Andrieu et al., 2016). These carbonate fossils are associated in many localities with ooids (e.g. Burgundy-Ardèche, France, Dromart et al., 1996; Lusitanian basin, Portugal, Azerêdo, 1998; Jura, France, Thiry-Bastien, 2002; United Arab Emirates, Hönig and John, 2015; northwestern Paris basin, France, Andrieu et al., 2016). The filtering carbonate production in neritic environments was mixed between heterozoan and microbial production (Andrieu et al., 2016) and dominated by grains rather than mud. At Murtinheira and Chaudon-Norante, the carbonate fraction is dominated by mud (Pavia, 1983; Suchéras-Marx et al., 2012) but these pelagic sections are the far-reaching end of the carbonate export thus too far to receive grains. Some of the localities recording a marked decrease in carbonate accumulation are also characterized by a relative sea-level rise that could explain local carbonate crisis due to drowning (e.g. Provence, France, Léonide et al., 2007; Morocco, Bodin et al., 2017). The effect of the drowning could have been more effective due to environmental perturbation such as eutrophication. Those conditions may have in turn promoted heterozoan over photozoan platforms which are very sensible to water eutrophication. However, heterozoan platforms are less efficient in carbonate production and thus may have been unable to keep-up in times of rising sea level or water eutrophication. Nevertheless, this carbonate crisis was not global and did not shut down all type of neritic carbonate production and export to the basin. Hence, a carbonate crisis may have contributed to the lower Bajocian positive CIE but was certainly not its main driver.

5.4.3. Data-model comparison

Comparing the $\delta^{13}C_{bulk\ carbonate}$ and $\delta^{13}C_{org}$ in different localities may help to further constrain the possible causes of the positive CIE using the box models proposed by Kump and Arthur (1999). The stratigraphic changes in $\delta^{13}C_{bulk\ carbonate}$ *vs* $\delta^{13}C_{org}$ seem to differ substantially between localities related to local conditions and differences in carbon sources, as mentioned in section 5.1. However, there are two patterns observed in the three sections shown in Fig. 8, where the $\delta^{13}C_{org}$ profile systematically exhibits a slightly larger positive CIE and an earlier

return to pre-excursion values (basal Propinquans ammonite Zone) than that recorded by $\delta^{13}C_{bulk\ carbonate}$. Such a decoupling is incompatible with a simple model of productivity increase driven by a sole increase in phosphate delivery rate to the ocean, which predicts a synchronous positive CIE in δ_{org} and δ_{carb} (model fig. 3 in Kump and Arthur, 1999). Our results and published data seem more consistent with a model of coupled increase in rate of riverine phosphate and weathered carbon delivery to the oceans (model fig. 9 in Kump and Arthur, 1999). In the model, the negative CIE results from the enhanced delivery of ^{13}C-depleted carbon from weathering, whereas the increase in organic carbon burial is rather related to the combined effects of higher riverine phosphate delivery initiating the positive CIE and a pCO_2 decrease. Consequently, this version of the model predicts first a ~-0.5 ‰ negative CIE similar to that observed across the Aalenian-Bajocian boundary, followed by a δ_{org} ~1.5 ‰ positive CIE synchronous with a δ_{carb} ~1 ‰ positive CIE. Thus, like for the early Bajocian positive CIE, the CIE amplitude is higher in δ_{org} than in δ_{carb}. Finally, the δ_{org} tends in the model to start decreasing back to pre-CIE values earlier than δ_{carb}, as observed in our sections.

The modelled CIE is driven by a pulse of increased organic matter burial, for which, as mentioned earlier, there is low evidence in the early Bajocian. Alternatively, an increase in organic carbon accumulation might have occurred in basins that have not been investigated yet for their TOC contents or that have since then disappeared. Such an organic matter burial forces a decrease in pCO_2 that would induce a cooling because of counter-greenhouse conditions. This alternative prediction is in line with the ~120 ppm pCO_2 decrease previously calculated for the early Bajocian between the Aalenian-Bajocian boundary and the Propinquans ammonite Zone (Bodin et al., 2020). This is also consistent with the ~0.5 ‰ increase in brachiopod $\delta^{18}O$ values at Murtinheira, which, if interpreted as reflecting only temperature changes, suggests a 2.5°C cooling (i.e., Ferreira et al., 2019) of bottom waters in the Propinquans ammonite Zone (Fig. 8). The isotopic data are not perfectly in line with the model in terms of magnitude, which depends on input rates and pCO_2 decrease; besides, according to this model a temperature decrease should rather have occurred in the Discites and Laeviuscula ammonite zones. This discrepancy could be explained by a potential CO_2 increase at the Aalenian-Bajocian boundary, as suggested by stomatal data from the Yorkshire coast (Hesselbo et al., 2003), which would have delayed the temperature decrease, or simply by the relatively low resolution of brachiopod data in this interval. According to bivalve $\delta^{18}O$ data from France, bottom water temperatures increased between Propinquans and Humphriesianum ammonite zones (Brigaud et al., 2009), which could support an increase in pCO_2 following the event of enhanced productivity and burial of organic matter (Kump and Arthur, 1999).

This ‘cool snap’ echoes previous observations based on fossil wood and glendonite occurrences (Philippe and Thevenard, 1996; Price, 1999; Rogov and Zakharov, 2010; Rogov

et al., 2023) suggesting a cooling in the Bajocian *sensu lato*, which would require further stratigraphic refinement. The CO_2 release at the Aalenian-Bajocian boundary related to global plate tectonic and Pacific Ocean plate production (Bartolini and Larson, 2001; Labails et al., 2010) may have induced a rapid warming (Gomez et al., 2009; Korte et al., 2015; Ferreira et al., 2019) at the origin of the increase in the rate of phosphate and weathering carbon release to the oceans from localized riverine input. However, the rate of delivery of fertilizing elements to the ocean was too slow to have an damaging impact like it occurred during the OAE 2 (i.e., Cenomanian-Turonian boundary). On the contrary, the fertilization promoted diversification and productivity of plankton in the early Bajocian event (Bartolini et al., 2019; Giraud et al., 2016).

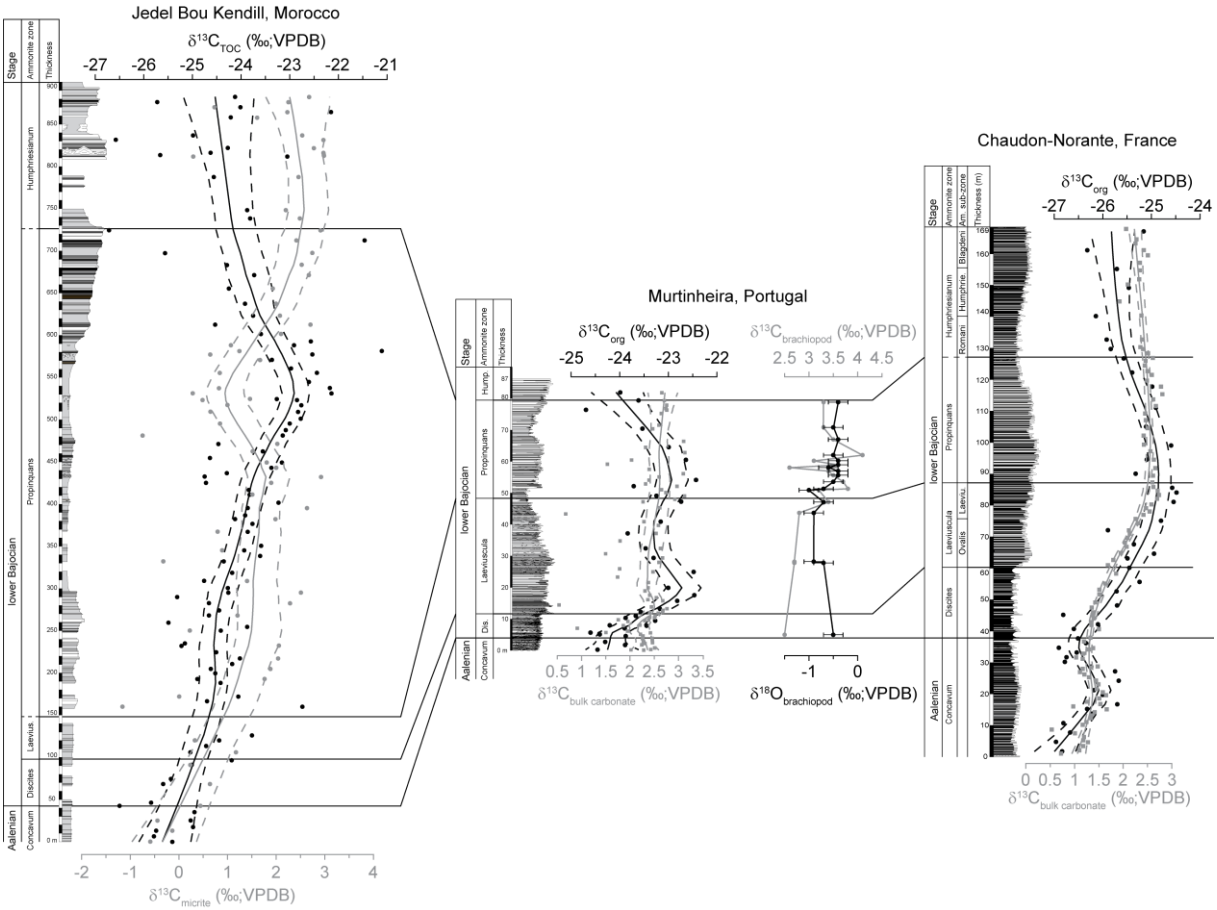

Fig. 8: $\delta^{13}C_{bulk\ carbonate}$ (grey squares; labelled $\delta^{13}C_{micrite}$ in Morocco following Bodin et al., 2017) versus $\delta^{13}C_{org}$ (black circles; labelled $\delta^{13}C_{TOC}$ in Morocco following Bodin et al., 2017) at Jedel Bou Kendill (Morocco; updated chronostratigraphic scheme in Bodin et al., 2020), Murtinheira (Portugal) and Chaudon-Norante (France) following a SW-NE transect. At Murtinheira, $\delta^{13}C_{brachiopod}$ (‰, VPDB; grey squares) and $\delta^{18}O_{brachiopod}$ (‰, VPDB; black circles) from Ferreira et al (2019) are plotted. The error bars for $\delta^{18}O_{brachiopod}$ are ±2σ analytical uncertainty.

The Aalenian to early Bajocian CIEs are very similar to the Weissert event in term of duration (Martinez et al., 2015), productivity increase (Gréselle et al., 2011; Duchamp-Alphonse et al., 2014; Mattioli et al., 2014; Shmeit et al., 2022) and possible cooling event (Barbarin et al., 2012; Cavaheiro et al., 2021; Wang et al., 2023). A biocalcification crisis has also been proposed for this specific event (Weissert et al., 1998) due to eutrophication related either to higher riverine detrital and nutrient input or from upwellings (see Shmeit et al., 2023 and references therein). Similar hypotheses were also proposed for the early Bajocian CIEs (i.e., Baumgartner, 2013). In both cases, widespread anoxia did not occur concomitant with the positive CIE. Thus, a similar cause – although unknown yet – can be at the origin of both these events. Erba et al. (2004) proposed a volcanic activity as possible cause but Shmeit et al. (2023) ruled out this hypothesis in Western Tethys). However, the Aalenian–Bajocian and early Valanginian have also noticeable differences. Firstly, the volcanic activity is clearly identified for the Valanginian CIE, whereas it remains poorly documented for the early Bajocian (Bartolini and Larson, 2001; Quirie et al., 2020). Arguably, a negative CIE (Hesselbo et al., 2003) occurred before the positive CIE in the Aalenian–Bajocian time interval, which is not the case in the Valanginian (Charbonnier et al., 2020). The Weissert event has been clearly documented worldwide, whereas the early Bajocian positive CIE has been documented only in Tethyan localities so far (Bodin et al., 2020). Finally, the early Bajocian is likely the most similar event to the Weissert event.

6. Conclusions

The early Bajocian was a time interval of important biologic, tectonic and climatic perturbations that have been clearly overseen because marine strata deposited during this event lack conspicuous black shale levels and evidence for anoxia. This time interval is also marked by a carbon cycle perturbation in the form of a long-lasting $\delta^{13}C$ positive excursion over the entire early Bajocian. In France at Chaudon-Norante and in Portugal at Murtinheira, the early Bajocian $\delta^{13}C$ positive excursion was previously recorded on bulk carbonate and biogenic calcite and is now also recorded in organic matter. This positive excursion reflects a long-lived and marked carbon cycle perturbation likely driven by an increase in organic carbon burial. The studied succession, however, indicate stable organic matter burial fluxes and deposition under steady oxygenation conditions, whereas an increase in erosion and productivity is supported by an increase in siliciclastic AR and PAR only in Murtinheira. The patterns seen in $\delta^{13}C_{bulk\ carbonate}$ and $\delta^{13}C_{org}$ are consistent with those previously described in box model simulating an increase in both riverine flux of phosphorus and inorganic carbon. The Bajocian carbon cycle perturbations fit particularly this solution combining both negative and positive excursions and a cooling period linked to pCO_2 decrease related to an increase in primary productivity. However, this model is clearly too simplistic. There are regional variations in

carbonate production with different producers on carbonate platforms (e.g., crinoids, microbialite, scleractinian) between platforms and in biological production with different marine organic producers and amount produced. Those geographical variations complexify the view of the global carbon and environmental perturbation based on too few sites of study.

The early Bajocian event was clearly different from the well-known Cenomanian-Turonian boundary $\delta^{13}C$ positive excursion and bears more similarities with the early Valanginian $\delta^{13}C$ positive excursion characterizing the Weissert event. Further geochemical data and especially more paleotemperature estimates and new sediment data ($CaCO_3$, TOC, P contents) outside the Tethys Ocean are needed to refine the Bajocian carbon cycle perturbation model. Moreover, volcanism (Mercury; Tellurium) and alteration tracers (clays analyses, chemical index of alteration) would help to dig further into the forcings at the base of the discussed CIEs.

Acknowledgments

BSM thanks Claudine Israel and Théo Mourier for samples decalcification at UJM. BSM thanks Chloé Morales for lodging in Lausanne. We thank Philippe Sorrel for help with palynomorph analyses. The analyses were partly funded by INSU TS SYSTER to EM. This manuscript is a contribution to CEREGE's team Climat.

Authors' contributions

BSM designed the study based on recommendations from FG, EM, GS and TA. BSM performed the phosphorus analyses in TA's lab at UNIL under the supervision of HK. AF and JS performed the $\delta^{13}C_{org}$ analyses at UNIL. JCM prepared the samples for OM observations at CEREGE. BSM and GS interpreted the results. BSM and GS wrote the manuscript with contributions from all authors.

Data availability

Data are curated by Pangaea, https://doi.pangaea.de/10.1594/PANGAEA.961170 for the Murtinheira section and https://doi.pangaea.de/10.1594/PANGAEA.961169 for the Chaudon-Norante section.

References

Adloff, M., Greene, S.E., Parkinson, I.J., Naafs, B.D.A., Preston, W., Ridgwell, A., Lunt, D.J., Castro Jiménez, J.M., & Monteiro, F.M. (2020). Unravelling the sources of carbon emissions at the onset of Oceanic Anoxic Event (OAE) 1a. *Earth and Planetary Science Letters*, 530, 115947. https://doi.org/10.1016/j.epsl.2019.115947

Aguado, R., O'Dogherty, L., & Sandoval, J. (2008). Fertility changes in surface waters during the Aalenian (mid-Jurassic) of the Western Tethys as revealed by calcareous nannofossils

and carbon-cycle perturbations. *Marine Micropaleontology*, *68*, 268-285. https://doi.org/10.1016/j.marmicro.2008.06.001

Aguado, R., O'Dogherty, L., & Sandoval, J. (2017). Calcareous nannofossil assemblage turnover in response to the Early Bajocian (Middle Jurassic) palaeoenvironmental changes in the Subbetic Basin. *Palaeogeography, Palaeoclimatology, Palaeoecology*, *472*, 128-145. http://doi.org/10.1016/j.palaeo.2017.01.044

Ait-Itto, F.-Z., Martinez, M., Price, G.D., & Ait Addi, A. (2018). Synchronization of the astronomical time scales in the Early Toarcian: A link between anoxia, carbon-cycle perturbation, mass extinction and volcanism. *Earth and Planetary Science Letters*, *493*, 1-11. https://doi.org/10.1016/j.epsl.2018.04.007

Al-Mojel, A., Dera, G., Razin, P., & Le Nindre, Y.-M. (2018). Carbon and oxygen isotope stratigraphy of Jurassic platform carbonates from Saudi Arabia: Implications for diagenesis, correlations and global paleoenvironmental changes. *Palaeogeography, Palaeoclimatology, Palaeoecology*, *511*, 388-402. https://doi.org/10.1016/j.palaeo.2018.09.005

Andrieu, S., Brigaud, B., Barbarand, J., Lasseur, E., & Saucède, T. (2016). Disentangling the control of tectonics, eustasy, trophic conditions and climate on shallow-marine carbonate production during the Aalenian–Oxfordian interval : From the western France platform to the western Tethyan domain. *Sedimentary Geology*, *345*, 54-84. https://doi.org/10.1016/j.sedgeo.2016.09.005

Aurell, M., Robles, S., Badenas, B., Rosales, I., Quesada, S., Meléndez, G., & Garcia-Ramos, J.C. (2003). Transgressive-regressive cycles and Jurassic palaeogeography of the northeast Iberia. *Sedimentary Geology*, *162*, 239-271. https://doi.org/10.1016/S0037-0738(03)00154-4

Azerêdo, A. (1998). Geometry and facies dynamics of Middle Jurassic carbonate ramp sandbodies, West-Central Portugal. In V. P. Wright & T. P. Burchette (Eds.), *Carbonate Ramps* (Vol. 149, p. 281-314). Geological Society, London, Special Publications. https://doi.org/10.1144/GSL.SP.1999.149.01.14

Baumgartner, P.O. (2013). Mesozoic radiolarites – accumulation as a function of sea surface fertility on Tethyan margins and in ocean basins. *Sedimentology*, *60*, 292-318. https://doi.org/10.1111/sed.12022

Barbarin, N., Bonin, A., Mattioli, E., Pucéat, E., Cappetta, H., Gréselle, B., Pittet, B., Vennin, E., & Joachimski, M. (2012). Evidence for a complex Valanginian nannoconid decline in the Vocontian basin (South East France). *Marine Micropaleontology*, *84-85*, 37-53. https://doi.org/10.1016/j.marmicro.2011.11.005

Barski, M., Matyja, B.A., Segit, T., & Wierzbowski, A. (2012). Early to Late Bajocian age of the “black flysch” (Szlachtowa Fm.) deposits: implications for the history and geological

structure of the Pieniny Klippen Belt, Carpathians. *Geological Quarterly*, *56*, 391-410. https://doi.org/10.7306/gq.1030

Bartolini, A., & Cecca, F. (1999). 20 My hiatus in the Jurassic of Umbria-Marche Apennines (Italy): Carbonate crisis due to eutrophication. *Comptes Rendus Académies des Sciences*, *329*, 587-595. https://doi.org/10.1016/S1251-8050(00)87215-8

Bartolini, A., & Larson, R.L. (2001). Pacific microplate and the Pangea supercontinent in the Early to Middle Jurassic. *Geology*, *29*, 735-738. https://doi.org/10.1130/0091-7613(2001)029<0735:PMATPS>2.0.CO;2

Bartolini, A., Baumgartner, P.O., & Hunziker, J.C. (1996). Middle and Late Jurassic carbon stable-isotope stratigraphy and radiolarite sedimentation of the Umbria-Marche Basin (Central Italy). *Eclogae Geologicae Helvetiae*, *89*, 811-844. https://doi.org/10.5169/seals-167925

Bartolini, A., Baumgartner, P.O., & Guex, J. (1999). Middle and Late Jurassic radiolarian palaeoecology versus carbon-isotope stratigraphy. *Palaeogeography, Palaeoclimatology, Palaeoecology*, *145*, 43-60. https://doi.org/10.1016/S0031-0182(98)00097-2

Bill, M., O'Dogherty, L., Guex, J., Baumgartner, P.O., & Masson, H. (2001). Radiolarite ages in Alpine-Mediterranean ophiolites: Constraints on the oceanic spreading and the Tethys-Atlantic connection. *Geological Society of America Bulletin*, *113*, 129-143. https://doi.org/10.1130/0016-7606(2001)113<0129:RAIAMO>2.0.CO;2

Blättler, C.L., Jenkyns, H.C., Reynard, L.M., & Henderson, G.M. (2011). Significant increases in global weathering during Oceanic Anoxic Events 1a and 2 indicated by calcium isotopes. *Earth and Planetary Science Letters*, *309*, 77-88. https://doi.org/10.1016/j.epsl.2011.06.029

Bodin, S., Hönig, M.R., Krencker, F.-N., Danisch, J., & Kabiri, L. (2017). Neritic carbonate crisis during the Early Bajocian: Divergent responses to a global environmental perturbation. *Palaeogeography, Palaeoclimatology, Palaeoecology*, *468*, 184-199. https://doi.org/10.1016/j.palaeo.2016.12.017

Bodin, S., Mau, M., Sadki, D., Danisch, J., Nutz, A., Krencker, F.-N., & Kabiri, L. (2020). Transient and secular changes in global carbon cycling during the early Bajocian event: Evidence for Jurassic cool climate episodes. *Global and Planetary Change*, *194*, 103287. https://doi.org/10.1016/j.gloplacha.2020.103287

Bomou, B., Adatte, T., Tantawy, A.A., Mort, H., Fleitmann, D., Huang, Y., & Föllmi, K.B. (2013). The expression of the Cenomanian-Turonian oceanic anoxic event in Tibet. *Palaeogeography, Palaeoclimatology, Palaeoecology*, *369*, 466-481. http://dx.doi.org/10.1016/j.palaeo.2012.11.011

BouDagher-Fadel, M. K. (2015). The Mesozoic planktonic foraminifera: The Late Triassic–Jurassic. In *Biostratigraphic and Geological Significance of Planktonic Foraminifera* (2e, Revised ed., p. 39-60). UCL Press. https://doi.org/10.2307/j.ctt1g69xwk.6

Boulila, S., Charbonnier, G., Spangenberg, J.E., Gardin, S., Galbrun, B., Briard, J., & Le Callonnec, L. (2020). Unraveling short- and long-term carbon cycle variations during the Oceanic Anoxic Event 2 from the Paris Basin Chalk. *Global and Planetary Change*, *186*, 103126. https://doi.org/10.1016/j.gloplacha.2020.103126

Brigaud, B., Durlet, C., Deconinck, J.-F., Vincent, B., Pucéat, E., Thierry, J., & Trouiller, A. (2009). Facies and climate/environmental changes recorded on a carbonate ramp: A sedimentological and geochemical approach on Middle Jurassic carbonates (Paris Basin, France). *Sedimentary Geology*, *222*, 181-206. https://doi.org/10.1016/j.sedgeo.2009.09.005

Cavalheiro, L., Wagner, T., Steinig, S., Bottini, C., Dummann, W., Esegbue, O., Gambacorta, G., Giraldo-Gómez, V., Farnsworth, A., Flögel, S., Hofmann, P., Lunt, D.J., Rethemeyer, J., Torricelli, S., & Erba, E. (2021). Impact of global cooling on Early Cretaceous high pCO_2 world during the Weissert Event. *Nature Communications*, *12*, 5411. https://doi.org/10.1038/s41467-021-25706-0

Charbonnier, G., Duchamp-Alphonse, S., Deconinck, J.F., Adatte, T., Spangenberg, J.E., Colin, C., & Föllmi, K.B. (2020). A global palaeoclimatic reconstruction for the Valanginian based on clay mineralogical and geochemical data. *Earth-Science Reviews*, *202*, 103092. https://doi.org/10.1016/j.earscirev.2020.

Cobianchi, M., Erba, E., & Pirini-Radrizzani, C. (1992). Evolutionary trends of calcareous nannofossil genera *Lotharingius* and *Watznaueria* during the Early and Middle Jurassic. *Memorie di Scienze Geologiche, Padova*, *43*, 19-25.

Cohen, K.M., Finney, S.C., Gibbard, P.L., & Fan, J.-X. (2013). The ICS International Chronostratigraphic Chart. *Episodes*, *36*, 199-204. https://doi.org/10.18814/epiiugs/2013/v36i3/002

Corbin, J.-C. (1994). *Evolution géochimique du Jurassique du Sud-Est de la France : influence du niveau marin et de la tectonique*. PhD thesis, Université Paris VI, 198 pp.

Dera, G., Brigaud, B., Monna, F., Laffont, R., Puceat, E., Deconinck, J.-F., Pellenard, P., Joachimski, M.M., & Durlet, C. (2011). Climatic ups and downs in a disturbed Jurassic world. *Geology*, *39*, 215-218. https://doi.org/10.1130/G31579.1

Danisch, J., Krencker, F.-N., Mau, M., Mattioli, E., Fauré, P., Alméras, Y., Nutz, A., Kabiri, L., El Ouali, M., & Bodin, S. (2021). Tracking a drowning unconformity up to the peritidal zone: Proximal expression of the early Bajocian carbonate crisis in Morocco. *Journal of African Earth Sciences*, *182*, 104300. https://doi.org/10.1016/j.jafrearsci.2021.104300

Dickens, G.R., O'Neil, J.R., Rea, D.K., & Owen, R.M. (1995). Dissociation of oceanic methane hydrate as a cause of the carbon isotope excursion at the end of the Paleogene. *Paleoceanography*, *10*, 965-971. https://doi.org/10.1029/95PA02087

Dromart, G., Allemand, P., Garcia, J.-P., & Robin, C. (1996). Variation cyclique de la production carbonatée au Jurassique le long d'un transect Bourgogne-Ardèche, Est-France. *Bulletin de la Société Géologique de France*, *167*, 423-433.

Duchamp-Alphonse, S., Gardin, S., & Bartolini, A. (2014). Calcareous nannofossil response to the Weissert episode (Early Cretaceous): Implications for palaeoecological and palaeoceanographic reconstructions. *Marine Micropaleontology*, *113*, 65-78. https://doi.org/10.1016/j.marmicro.2014.10.002

Eldrett, J.S., Ma, C., Bergman, S.C., Lutz, B., Gregory, F.J., Dodsworth, P., Phipps, M., Hardas, P., Minisini, D., Ozkan, A., Ramezani, J., Bowring, S.A., Kamo, S.L., Ferguson, K., Macaulay, C., & Kelly, A.E. (2015). An astronomically calibrated stratigraphy of the Cenomanian, Turonian and earliest Coniacian from the Cretaceous Western Interior Seaway, USA: Implications for global chronostratigraphy. *Cretaceous Research*, *56*, 316-344. https://doi.org/10.1016/j.cretres.2015.04.010

Erba, E. (1990). Calcareous nannofossil biostratigraphy of some Bajocian sections from the Digne area (SE France). *Memorie Descrittive Della Carta Geologica d'Italia XL*, 237-256.

Erba, E. (2004). Calcareous nannofossils and Mesozoic oceanic anoxic events. *Marine Micropaleontology*, *52*, 85-106. https://doi.org/10.1016/j.marmicro.2004.04.007

Erba, E., & Tremolada, F. (2004). Nannofossil carbonate fluxes during the Early Cretaceous: Phytoplankton response to nutrification episodes, atmospheric CO_2, and anoxia. *Paleoceanography*, *19*, PA1008. https://doi.org/10.1029/2003PA000884

Erba, E., Bartolini, A., & Larson, R.L. (2004). Valanginian Weissert oceanic anoxic event. *Geology*, *32*, 149-152. https://doi.org/10.1130/G20008.1

Erba, E., Gambacorta, G., & Tiepolo, M. (2019). The Lower Bajocian Gaetani level: Lithostratigraphic marker of a potential oceanic anoxic event. *Rivista Italiana di Paleontologia e Stratigrafia*, *125*, 219-230. https://doi.org/10.13130/2039-4942/11390

Fantasia, A., Mattioli, E., Spangenberg, J.E., Adatte, T., Bernárdez, E., Ferreira, J., Thibault, N., Krencker, F.-N., & Bodin, S., (2022). The middle-late Aalenian event: A precursor of the Mesozoic Marine Revolution. *Global and Planetary Change, 208*, 103705. https://doi.org/10.1016/j.gloplacha.2021.103705

Fernandez-Lopez, S., Henriques, M.H., Mouterde, R., Rocha, R.B., & Sadki, D. (1988). Le Bajocien inférieur du Cap Mondego (Portugal) - Essai de biozonation. In *2nd International Symposium on Jurassic Stratigraphy* (p. 301-313). Lisboa.

Fernandez-Lopez, S., Pavia, G., Erba, E., Guiomar, M., Henriques, M.H., Lanza, R., Mangold, C., Morton, N., Olivero, D., & Tiraboschi, D. (2009). The Global Boundary Stratotype Section and Point (GSSP) for base of the Bathonian Stage (Middle Jurassic), Ravin du Bès Section, SE France. *Episodes*, *32*, 222-248. https://doi.org/10.1007/s00015-009-1317-1

Ferreira, J., Mattioli, E., Sucherás-Marx, B., Giraud, F., Duarte, L.V., Pittet, B., Suan, G., Hassler, A., & Spangenberg, J.E. (2019). Western Tethys Early and Middle Jurassic calcareous nannofossil biostratigraphy. *Earth-Science Reviews*, *197*, 102908. https://doi.org/10.1016/j.earscirev.2019.102908

Friedrich, O., Norris, R.D., & Erbacher, J. (2012). Evolution of middle to Late Cretaceous oceans-A 55 m.y. record of Earth's temperature and carbon cycle. *Geology*, *40*, 107-110. https://doi.org/10.1130/G32701.1

Giraud, F., Mattioli, E., López-Otálvaro, G.E., Lécuyer, C., Suchéras-Marx, B., Alméras, Y., Martineau, F., Arnaud-Godet, F., & de Kænel, E. (2016). Deciphering processes controlling mid-Jurassic coccolith turnover. *Marine Micropaleontology*, *125*, 36-50. https://doi.org/10.1016/j.marmicro.2016.03.001

Gomez, J.J., Canales, M.L., Ureta, S., & Goy, A. (2009). Palaeoclimatic and biotic changes during the Aalenian (Middle Jurassic) at the southern Laurasian Seaway (Basque–Cantabrian Basin, northern Spain). *Palaeogeography, Palaeoclimatology, Palaeoecology*, *275*, 14-27. https://doi.org/10.1016/j.palaeo.2009.01.009

Gradstein, F.M., Ogg, J.G., Schmitz, M.D., & Ogg, G.M. (2020). *Geological time scale 2020* (Vol. 1-2, 1357 pp.). Elsevier, Amsterdam. https://doi.org/10.1016/C2020-1-02369-3

Gréselle, B., Pittet, B., Mattioli, E., Joachimski, M., Barbarin, N., Riquier, L., Reboulet, S., & Pucéat, E. (2011). The Valanginian isotope event: A complex suite of palaeoenvironmental perturbations. *Palaeogeography, Palaeoclimatology, Palaeoecology*, *306*, 41-57. https://doi.org/10.1016/j.palaeo.2011.03.027

Hammer, Ø., Harper, D.A.T., & Ryan, P.D. (2001). PAST: paleontological statistics software package for education and data analysis. *Palaeontologia Electronica*, *4*, 1-9. http://palaeo-electronica.org/2001_1/past/issue1_01.htm

Henriques, M.H., Gardin, S., Gomes, C.R., Soares, A.F., Rocha, R.B., Marques, J.F., Lapa, M.R., & Montenegro, J.D. (1994). The Aalenian-Bajocian boundary at Cabo Mondego (Portugal). In Cresta, S. & G. Pavia (Eds.), *3rd International Meeting on Aalenian and Bajocian Stratigraphy* (p. 63-77). Miscellanea Servizio Geologico Nazionale, Marrakesh.

Hesselbo, S.P., Grocke, D.R., Jenkyns, H.C., Bjerrum, C.J., Farrimond, P., Morgans-Bell, H.S., & Green, O.R. (2000). Massive dissociation of gas hydrate during a Jurassic oceanic anoxic event. *Nature*, *406*, 392-395. https://doi.org/10.1038/35019044

Hesselbo, S.P., Morgans-Bell, H.S., McElwain, J.C., Rees, P.M., Robinson, S.A., & Ross, C.E. (2003). Carbon-cycle perturbation in the middle Jurassic and accompanying changes in the terrestrial paleoenvironment. *The Journal of Geology*, *111*, 259-276. https://doi.org/10.1086/373968

Hönig, M.R., & John, C.M. (2015). Sedimentological and isotopic heterogeneities within a Jurassic carbonate ramp (UAE) and implications for reservoirs in the Middle East. *Marine*

and Petroleum Geology, *68*, Part A, 240-257. http://dx.doi.org/10.1016/j.marpetgeo.2015.08.029

Huang, C., & Hesselbo, S.P. (2014). Pacing of the Toarcian Oceanic Anoxic Event (Early Jurassic) from astronomical correlation of marine sections. *Gondwana Research*, *25*, 1348-1356. http://dx.doi.org/10.1016/j.gr.2013.06.023

Ikeda, M., Bôle, M., & Baumgartner, P.O. (2016). Orbital-scale changes in redox condition and biogenic silica/detrital fluxes of the Middle Jurassic Radiolarite in Tethys (Sogno, Lombardy, N-Italy): Possible link with glaciation? *Palaeogeography, Palaeoclimatology, Palaeoecology*, *457*, 247-257. https://doi.org/10.1016/j.palaeo.2016.06.009

Imlay, R.W. (1976). Middle Jurassic (Bajocian and Bathonian) ammonites from northern Alaska. *Geological Survey Professional Paper*, *854*, 1-22. https://doi.org/10.3133/pp854

Jarvis, I., Lignum, J.S., Gröcke, D.R., Jenkyns, H.C., & Pearce, M.A. (2011). Black shale deposition, atmospheric CO_2 drawdown, and cooling during the Cenomanian-Turonian Oceanic Anoxic Event. Paleoceanography 26, PA3201. https://doi.org/10.1029/2010PA002081

Jenkyns, H.C., Jones, C.E., Gröcke, D.R., Hesselbo, S.P., & Parkinson, P.N. (2002). Chemostratigraphy of the Jurassic System: applications, limitations and implications for palaeoceanography. *Journal of the Geological Society, London*, *159*, 351-378. https://doi.org/10.1144/0016-764901-130

Kendall, C.G.St.C., Chiarenzelli, J., & Hassan, S.H. (2009). World source rock potential through geological time: A function of basin restriction, nutrient level, sedimentation rate, and sea-level rise. *AAPG Search and Discovery Article #40472*. https://doi.org/10.13140/RG.2.2.16943.69288

Korte, C., Hesselbo, S.P., Ullmann, C.V., Dietl, G., Ruhl, M., Schweigert, G., & Thibault, N. (2015). Jurassic climate mode governed by ocean gateway. *Nature Communications*, *6*, 10015. https://doi.org/10.1038/ncomms10015

Kump, L.R., & Arthur, M.A. (1999). Interpreting carbon-isotope excursions: carbonates and organic matter. *Chemical Geology*, *161*, 181-198. https://doi.org/10.1016/S0009-2541(99)00086-8

Labails, C., Olivet, J.-L., Aslanian, D., & Roest, W.R. (2010). An alternative early opening scenario for the Central Atlantic Ocean. *Earth and Planetary Science Letters*, *297*, 355-368. https://doi.org/10.1016/j.epsl.2010.06.024

Larson, R.L., & Erba, E. (1999). Onset of the Mid-Cretaceous greenhouse in the Barremian-Aptian: Igneous events and the biological, sedimentary, and geochemical responses. *Paleoceanography*, *14*, 663-678. https://doi.org/10.1029/1999PA900040

Léonide, P., Floquet, M., & Villier, L. (2007). Interaction of tectonics, eustasy, climate and carbonate production on the sedimentary evolution of an early/middle Jurassic extensional

basin (Southern Provence Sub-basin,SE France). *Basin Research*, *19*, 125-152. https://doi.org/10.1111/j.1365-2117.2007.00316.x

Ma, C., Meyers, S.R., Sageman, B.B., Singer, B.S., & Jicha, B.R. (2014). Testing the astronomical time scale for oceanic anoxic event 2, and its extension into Cenomanian strata of the Western Interior Basin (USA). *Geological Society of America Bulletin*, *126*, 974-989. https://doi.org/10.1130/B30922.1

Malinverno, A., Erba, E., & Herbert, T.D. (2010). Orbital tuning as an inverse problem: Chronology of the early Aptian oceanic anoxic event 1a (Selli Level) in the Cismon APTICORE. *Paleoceanography*, *25*, PA2203. https://doi.org/10.1029/2009PA001769

Martinez, M., Deconinck, J.-F., Pellenard, P., Riquier, L., Company, M., Reboulet, S., & Moiroud, M. (2015). Astrochronology of the Valanginian–Hauterivian stages (Early Cretaceous): Chronological relationships between the Paraná–Etendeka large igneous province and the Weissert and the Faraoni events. *Global and Planetary Change*, *131*, 158-173. https://doi.org/10.1016/j.gloplacha.2015.06.001

Matsumoto, H., Coccioni, R., Frontalini, F., Shirai, K., Jovane, L., Trindade, R., Savian, J.F., Kuroda, J. (2022). Mid-Cretaceous marine Os isotope evidence for heterogeneous cause of oceanic anoxic events. *Nature Communications*, 13, 239. https://doi.org/10.1038/s41467-021-27817-0

Mattioli, E., Pittet, B., Riquier, L., & Grossi, V. (2014). The mid-Valanginian Weissert Event as recorded by calcareous nannoplankton in the Vocontian Basin. *Palaeogeography, Palaeoclimatology, Palaeoecology*, *414*, 472-485. http://dx.doi.org/10.1016/j.palaeo.2014.09.030

Molina, J.M., Reolid, M., & Mattioli, E. (2018). Thin-shelled bivalve buildup of the lower Bajocian, South Iberian paleomargin: development of opportunists after oceanic perturbations. *Facies*, *64*, 19. https://doi.org/10.1007/s10347-018-0532-5

Monteiro, F.M., Pancost, R.D., Ridgwell, A., & Donnadieu, Y. (2012). Nutrients as the dominant control on the spread of anoxia and euxinia across the Cenomanian-Turonian oceanic anoxic event (OAE2): Model-data comparison. *Paleoceanography*, *27*, PA4209. https://doi.org/10.1029/2012pa002351

Mort, H.P., Adatte, T., Föllmi, K.B., Keller, G., Steinmann, P., Matera, V., Berner, Z., & Stüben, D. (2007). Phosphorus and the roles of productivity and nutrient recycling during oceanic anoxic event 2. *Geology*, *35*, 483-486. https://doi.org/10.1130/g23475a.1

O'Dogherty, L., Sandoval, J., Bartolini, A., Bruchez, S., Bill, M., & Guex, J. (2006). Carbon-isotope stratigraphy and ammonite faunal turnover for the Middle Jurassic in the Southern Iberian palaeomargin. *Palaeogeography, Palaeoclimatology, Palaeoecology*, *239*, 311-333. https://doi.org/10.1016/j.palaeo.2006.01.018

Olivero, D. (1994). La trace fossile *Zoophycos* du Jurassique du Sud-Est de la France. Signification paléoenvironnementale. *Documents des laboratoires de géologie de Lyon*, *129*, 329 pp.

Pacton, M., Gorin, G.E., & Vasconcelos, C. (2011). Amorphous organic matter — Experimental data on formation and the role of microbes. *Review of Palaeobotany and Palynology*, *166*, 253-267. https://doi.org/10.1016/j.revpalbo.2011.05.011

Papadomanolaki, N.M., van Helmond, N.A.G.M., Pälike, H., Sluijs, A.,& Slomp, C.P. (2022) Quantifying volcanism and organic carbon burial across Oceanic Anoxic Event 2. *Geology*, *50*, 511-515. https://doi.org/10.1130/G49649.1

Pavia, G. (1983). Ammoniti e biostratigrafia del Baiociano inferiore di Digne (Francia SE, Dip. Alpes-Haute-Provence). *Monografie Museo Regionale di Scienze Naturali, Torino*, 254 pp.

Pavia, G., & Enay, R. (1997). Definition of the Aalenian-Bajocian Stage boundary. *Episodes*, *20*, 16-22. https://doi.org/10.18814/epiiugs/1997/v20i1/004

Philippe, M., & Thevenard, F. (1996). Distribution and palaeocology of the Mesozoic wood genus *Xenoxylon*: palaeoclimatological implications for the Jurassic of Western Europe. *Review of Palaeobotany and Palynology*, *91*, 353-370. https://doi.org/10.1016/0034-6667(95)00067-4

Pogge von Strandmann, P.A.E., Jenkyns, H.C., & Woodfine, R.G. (2013). Lithium isotope evidence for enhanced weathering during Oceanic Anoxic Event 2. *Nature Geoscience*, *6*, 668-672. https://doi.org/10.1038/ngeo1875

Price, G.D. (1999). The evidence and implications of polar ice during the Mesozoic. *Earth-Science Reviews*, *48*, 183-210. https://doi.org/10.1016/S0012-8252(99)00048-3

Quirie, A.K., Schofield, N., Jolley, D.W., Archer, S.G., Hole, M.J., Hartley, A., Watson, D., Burgess, R., Pugsley, J.H., Underhill, J.R., & Holford, S.P. (2020). Palaeogeographical evolution of the Rattray Volcanic Province, Central North Sea. *Journal of the Geological Society*, *177*, 718–737. https://doi.org/10.1144/jgs2019-182

Raucsik, B. (1999). Clay mineralogy of the Komló Calcareous Marl Formation, Bajocian, Mecsek Mountains, Hungary. *Acta Geologica Hungarica*, *42*, 379-400.

Raucsik, B., Demény, A., Borbély-Kiss, I., & Szabó, G. (2001). Monsoon-like climate during the Bajocian. Clay mineralogical and geochemical study on a limestone/marl alternation (Komló Calcareous Marl Formation, Mecsek Mountains, Southern Hungary). *Hantkeniana*, *3*, 149-176.

Rogov, M.A., & Zakharov, V.A. (2010). Jurassic and Lower Cretaceous glendonites occurrences and their implication for Arctic paleoclimatic reconstructions and stratigraphy. *Earth Science Frontiers*, *Special Issue*, *17*, 345-347.

Rogov, M., Ershova, V., Gaina, C., Vasileva, K., Mikhailova, K., & Krylov, A. (2023). Glendonites throughout the Phanerozoic. *Earth-Science Reviews*, *241*, 104430. https://dx.doi.org/10.1016/j.earscirev.2023.104430

Ruebsam, W., Münzberger, P.& Schwark, L. (2014). Chronology of the Early Toarcian environmental crisis in the Lorraine Sub-Basin (NE Paris Basin). *Earth and Planetary Science Letters*, *404*, 273-282. http://dx.doi.org/10.1016/j.epsl.2014.08.005

Ruget-Perrot, C. (1961). Etudes stratigraphiques sur le Dogger et le Malm inférieur du Portugal au Nord du Tage. *Memoria Serviços Geologicos de Portugal*, *7*, 197 pp.

Schlanger, S. O., Arthur, M. A., Jenkyns, H. C., & Scholle, P. A. (1987). The Cenomanian-Turonian oceanic anoxic event, I. Stratigraphy and distribution of organic carbon-rich beds and the marine $\delta^{13}C$ excursion. In J. Brooks & A. J. Fleet (Eds.), *Marine petroleum source rocks* (Vol. 26, p. 371-399). Geological Society Special Publications. https://doi.org/10.1144/GSL.SP.1987.026.01.24

Shmeit, M., Chauvel, C., Giraud, F., Jaillard, E., Reboulet, S., Masrour, M., Spangenberg, J.E., & El-Samrani, A., (2023). Geochemical and radiogenic isotope records of the Weissert Event in south Tethyan sediments. *Journal of the Geological Society*, *180*, jgs2022-023. https://doi.org/10.1144/jgs2022-023

Shmeit, M., Giraud, F., Jaillard, E., Reboulet, S., Masrour, M., Spangenberg, J.E., & El-Samrani, A., (2022). The Valanginian Weissert Event on the south Tethyan margin: A dynamic paleoceanographic evolution based on the study of calcareous nannofossils. *Marine Micropaleontology*, *175*, 102134. https://doi.org/10.1016/j.marmicro.2022.102134

Suan, G., Föllmi, K.B., Adatte, T., Bomou, B., Spangenberg, J.E., & van de Schootbrugge, B. (2012). Major environmental change and bonebed genesis prior to the Triassic-Jurassic mass extinction. *Journal of the Geological Society, London*, *169*, 191-200. https://doi.org/10.1144/0016-76492011-045

Suan, G., Mattioli, E., Pittet, B., Lécuyer, C., Suchéras-Marx, B., Duarte, L.V., Philippe, M., Reggiani, L., & Martineau, F. (2010). Secular environmental precursors to Early Toarcian (Jurassic) extreme climate changes. *Earth and Planetary Science Letters*, *290*, 448-458. https://doi.org/10.1016/j.epsl.2009.12.047

Suan, G., Pittet, B., Bour, I., Mattioli, E., Duarte, L.V., & Mailliot, S. (2008). Duration of the Early Toarcian carbon isotope excursion deduced from spectral analysis: Consequence for its possible causes. *Earth and Planetary Science Letters*, *267*, 666-679. https://doi.org/10.1016/j.epsl.2007.12.017

Suan, G., van de Schootbrugge, B., Adatte, T., Fiebig, J., & Oschmann, W. (2015). Calibrating the magnitude of the Toarcian carbon cycle perturbation. *Paleoceanography*, *30*, 2014PA002758. https://doi.org/10.1002/2014PA002758

Suchéras-Marx, B., Giraud, F., Fernandez, V., Pittet, B., Lécuyer, C., Olivero, D., & Mattioli, E. (2013). Duration of the Early Bajocian and the associated $\delta^{13}C$ positive excursion based on cyclostratigraphy. *Journal of the Geological Society, London*, *170*, 107-118. https://doi.org/10.1144/jgs2011-133

Suchéras-Marx, B., Giraud, F., Mattioli, E., & Escarguel, G. (2015). Paleoenvironmental and paleobiological origins of coccolithophorid genus *Watznaueria* emergence during the Late Aalenian-Early Bajocian. *Paleobiology*, *41*, 415-435. https://doi.org/10.1017/pab.2015.8

Suchéras-Marx, B., Giraud, F., Mattioli, E., Gally, Y., Barbarin, N., & Beaufort, L. (2014). Middle Jurassic coccolith fluxes: A novel approach by automated quantification. *Marine Micropaleontology*, *111*, 15-25. https://doi.org/10.1016/j.marmicro.2014.06.002

Suchéras-Marx, B., Guihou, A., Giraud, F., Lécuyer, C., Allemand, P., Pittet, B., & Mattioli, E. (2012). Impact of the Middle Jurassic diversification of *Watznaueria* (coccolith-bearing algae) on the carbon cycle and $\delta^{13}C$ of bulk marine carbonates. *Global and Planetary Change*, *86-87*, 92-100. https://doi.org/10.1016/j.gloplacha.2012.02.007

Swart, P.K., & Eberli, G. (2005). The nature of the $\delta^{13}C$ of periplatform sediments: Implications for stratigraphy and the global carbon cycle. *Sedimentary Geology*, *175*, 115-129. https://doi.org/10.1016/j.sedgeo.2004.12.029

Thiry-Bastien, P. (2002). *Stratigraphie séquentielle des calcaires bajociens de l'Est de la France (Jura-Bassin de Paris)*. PhD thesis, Université Claude Bernard Lyon1, Villeurbanne, 407 pp.

Trabucho Alexandre, J., Tuenter, E., Henstra, G.A., van der Zwan, K.J., van de Wal, R.S.W., Dijkstra, H.A., & de Boer, P.L. (2010). The mid-Cretaceous North Atlantic nutrient trap: Black shales and OAEs. *Paleoceanography*, *25*, PA4201. https://doi.org/10.1029/2010pa001925

Tyson, R.V. (1995). Bulk geochemical characterization and classification of organic matter: Stable carbon isotopes ($\delta^{13}C$). In *Sedimentary Organic Matter* (p. 395–416). Springer, Netherlands. https://doi.org/10.1007/978-94-011-0739-6_23

Vincent, E., & Berger, W.H. (1985). Carbon Dioxide and Polar Cooling in the Miocene : The Monterey Hypothesis. In E.T. Sundquist & W.S. Broecker (Eds.), *The Carbon Cycle and Atmospheric CO_2: Natural Variations Archean to Present* (p. 455-468). Geophysical Monograph Series.

Voigt, S., Erbacher, J., Mutterlose, J., Weiss, W., Westerhold, T., Wiese, F., Wilmsen, M., & Wonik, T. (2008). The Cenomanian – Turonian of the Wunstorf section – (North Germany): global stratigraphic reference section and new orbital time scale for Oceanic Anoxic Event 2. *Newsletters on Stratigraphy*, *43*, 65-89. https://doi.org/10.1127/0078-0421/2008/0043-0065

Wang, T., He, S., Zhang, Q., Ding, L., Farnsworth, A., Cai, F., Wang, C., Xie, J., Li, G., Sheng, J., & Yue, Y. (2023). Ice Sheet Expansion in the Cretaceous Greenhouse World. *Fundamental Research*. https://doi.org/10.1016/j.fmre.2023.05.005

Weissert, H., Lini, A., Föllmi, K.B., & Kuhn, O. (1998). Correlation of Early Cretaceous carbon isotope stratigraphy and platform drowning events: a possible link? *Palaeogeography, Palaeoclimatology, Palaeoecology*, *137*, 189-203. https://doi.org/10.1016/S0031-0182(97)00109-0

Westermann, S., Stein, M., Matera, V., Fiet, N., Fleitmann, D., Adatte, T., & Föllmi, K.B. (2013). Rapid changes in the redox conditions of the western Tethys Ocean during the early Aptian oceanic anoxic event. *Geochimica et Cosmochimica Acta*, *121*, 467-486. http://doi.org/10.1016/j.gca.2013.07.023

Wiggan, N.J., Riding, J.B., & Franz, M. (2017). Resolving the Middle Jurassic dinoflagellate radiation: The palynology of the Bajocian of Swabia, southwest Germany. *Review of Palaeobotany and Palynology*, *238*, 55-87. https://doi.org/10.1016/j.revpalbo.2016.11.010

Wiggan, N.J., Riding, J.B., Fensome, R.A., & Mattioli, E. (2018). The Bajocian (Middle Jurassic): A key interval in the early Mesozoic phytoplankton radiation. *Earth-Science Reviews*, *180*, 126-146. https://doi.org/10.1016/j.earscirev.2018.03.009

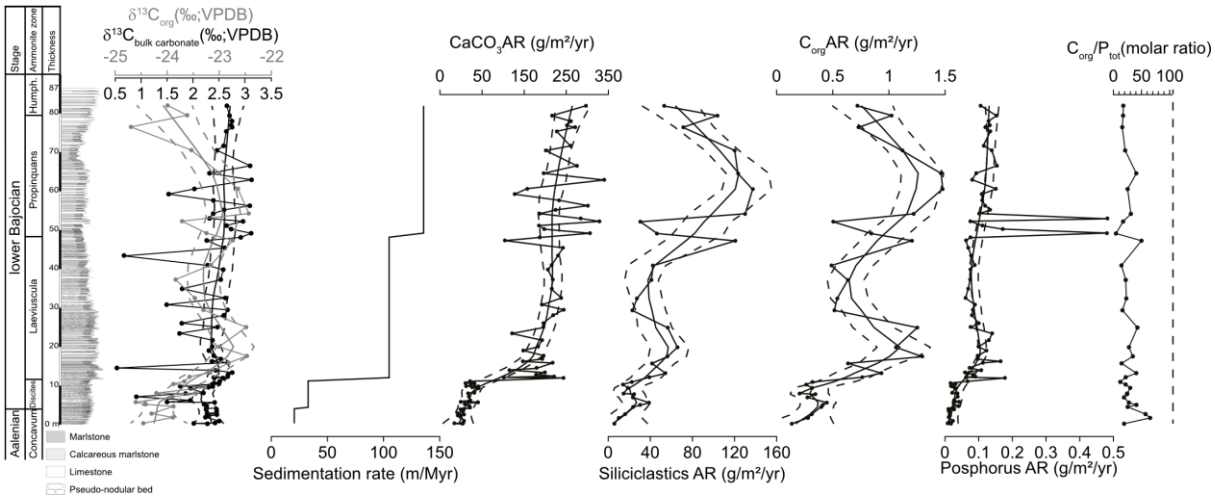

Supplementary Fig. 1: Stratigraphic changes in sedimentation rate at Murtinheira (based on Gradstein et al. (2020) age model) and the resulting $CaCO_3$ accumulation rates (AR; g/m²/yr), Siliciclastic AR (g/m²/yr), C_{org} AR (g/m²/yr), and phosphorus AR (g/m²/yr).

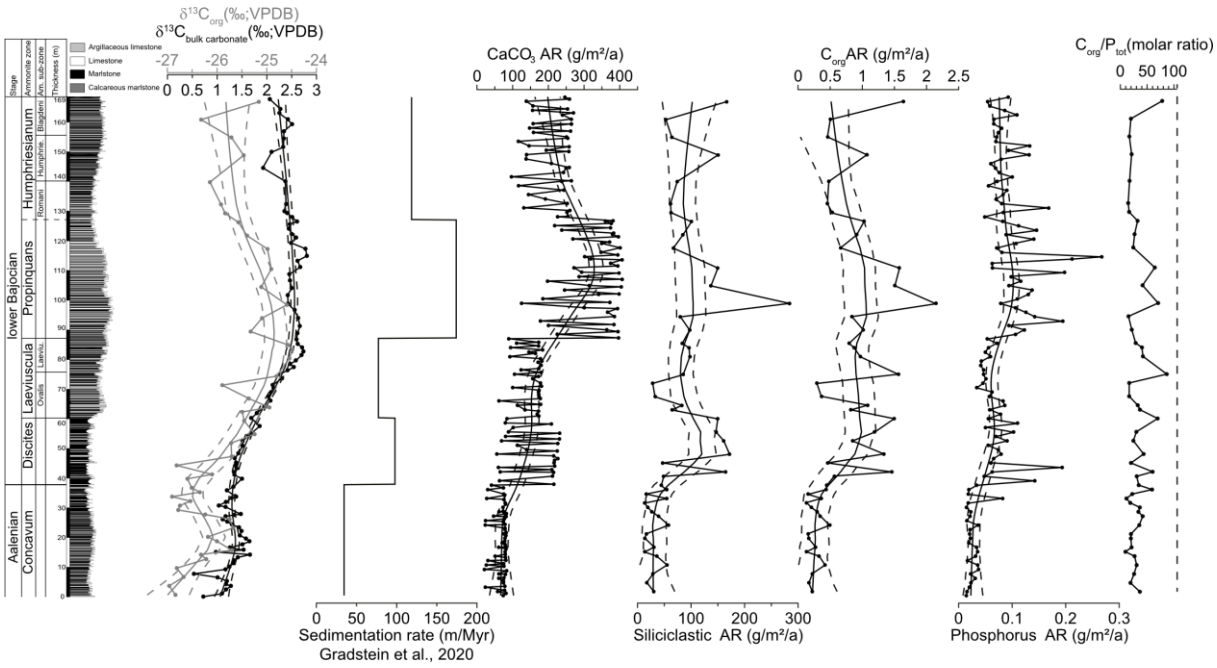

Supplementary Fig. 2: Stratigraphic changes in sedimentation rate at Chaudon-Norante (based on Gradstein et al. (2020) age model) and the resulting $CaCO_3$ accumulation rates (AR; g/m²/yr), Siliciclastic AR (g/m²/yr), C_{org} AR (g/m²/yr), and phosphorus AR (g/m²/yr).

Aalenian
Bajocian
Concavum
Discites
Laeviuscula
Propinquans
Humphriesianum

Marlstone
Calcareous marlstone
Limestone
Pseudo-nodular bed

Supplementary Fig. 3: Stratigraphic log of Murtinheira section, Portugal with sample localization.

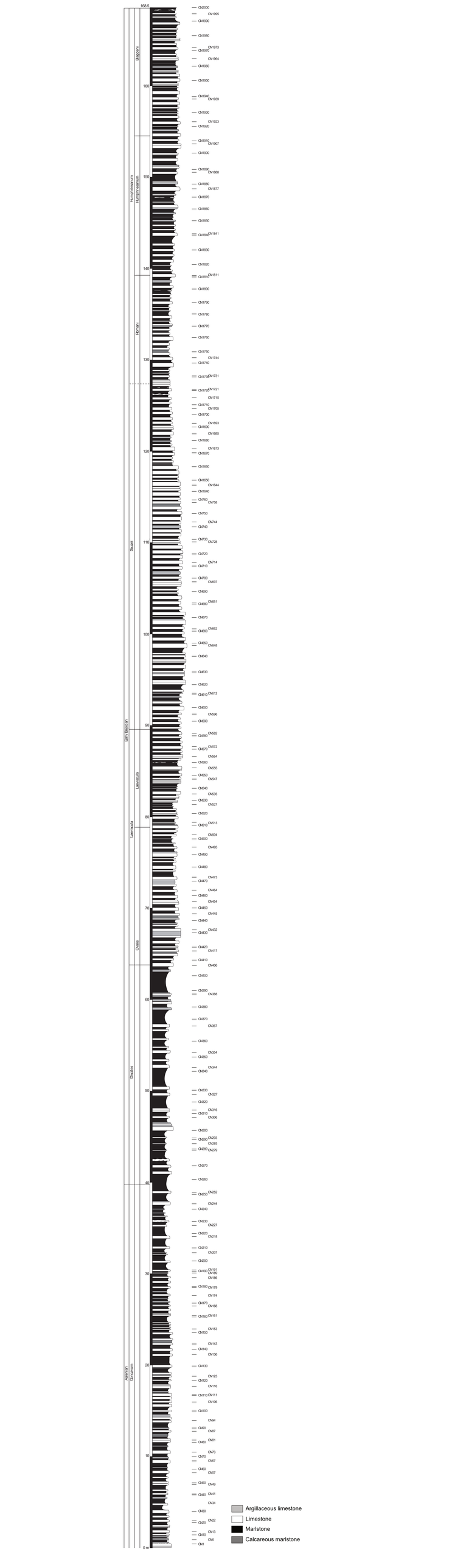
168.5
160
150
140
130
120
110
100
90
80
70
60
50
40
30
20
10
0 m
Aalenian
Toarcian
Pliensbachian
Sinemurian
Hettangian
Rhaetian
Norian
Carnian
Ladinian
Anisian
Olenekian
Induan
Changhsingian
Wuchiapingian
Capitanian
Wordian
Roadian
Kungurian
Artinskian
Sakmarian
Asselian
Gzhelian
Kasimovian
Moscovian
Bashkirian
Serpukhovian
Visean
Tournaisian
Famennian
Frasnian
Givetian
Eifelian
Emsian
Pragian
Lochkovian
Pridoli
Ludlow
Wenlock
Llandovery
Hirnantian
Katian
Sandbian
Darriwilian
Dapingian
Floian
Tremadocian
Stage 10
Furongian
Series 3
Series 2
Cambrian
Ediacaran
Cryogenian
Tonian
Stenian
Ectasian
Calymmian
Statherian
Orosirian
Rhyacian
Siderian
Neoarchean
Mesoarchean
Paleoarchean
Eoarchean
Hadean
Bajocian
Humphriesianum
Humphriesianum
Romani
Bauzei
Early Oxfordian
Lamberti
Lamberti
Lewisiceltis
Lewisiceltis
Ovalis
Ovalis
Discites
Discites
Aalenian
Concavum
CN2000
CN1995
CN1990
CN1980
CN1973
CN1970
CN1964
CN1960
CN1950
CN1940
CN1939
CN1930
CN1923
CN1920
CN1910
CN1907
CN1900
CN1890
CN1888
CN1880
CN1877
CN1870
CN1860
CN1850
CN1840
CN1841
CN1830
CN1820
CN1810
CN1811
CN1800
CN1790
CN1780
CN1770
CN1760
CN1750
CN1744
CN1740
CN1730
CN1731
CN1720
CN1721
CN1715
CN1710
CN1705
CN1700
CN1693
CN1690
CN1685
CN1680
CN1673
CN1670
CN1660
CN1650
CN1644
CN1640
CN1760
CN758
CN750
CN744
CN740
CN730
CN728
CN720
CN714
CN710
CN700
CN697
CN690
CN681
CN670
CN662
CN660
CN648
CN640
CN630
CN620
CN612
CN600
CN596
CN590
CN582
CN570
CN572
CN564
CN560
CN555
CN550
CN547
CN540
CN535
CN530
CN527
CN520
CN513
CN504
CN500
CN495
CN490
CN480
CN473
CN470
CN464
CN460
CN454
CN450
CN445
CN440
CN432
CN430
CN420
CN417
CN410
CN406
CN400
CN390
CN388
CN380
CN370
CN367
CN360
CN354
CN350
CN344
CN340
CN330
CN327
CN320
CN316
CN310
CN306
CN300
CN293
CN285
CN279
CN270
CN260
CN252
CN250
CN244
CN240
CN230
CN227
CN220
CN218
CN210
CN207
CN200
CN191
CN189
CN186
CN179
CN174
CN170
CN168
CN161
CN153
CN150
CN143
CN140
CN136
CN130
CN123
CN120
CN116
CN110
CN111
CN106
CN100
CN94
CN90
CN87
CN80
CN81
CN73
CN70
CN67
CN60
CN57
CN50
CN49
CN40
CN41
CN34
CN30
CN25
CN22
CN16
CN13
CN6
CN1
Argillaceous limestone
Limestone
Marlstone
Calcareous marlstone

Supplementary Fig. 4: Stratigraphic log of Chaudon-Norante section, France with sample localization.